SPECIAL PAPER 10

TECTONIC ROTATION OF THE OREGON WESTERN CASCADES

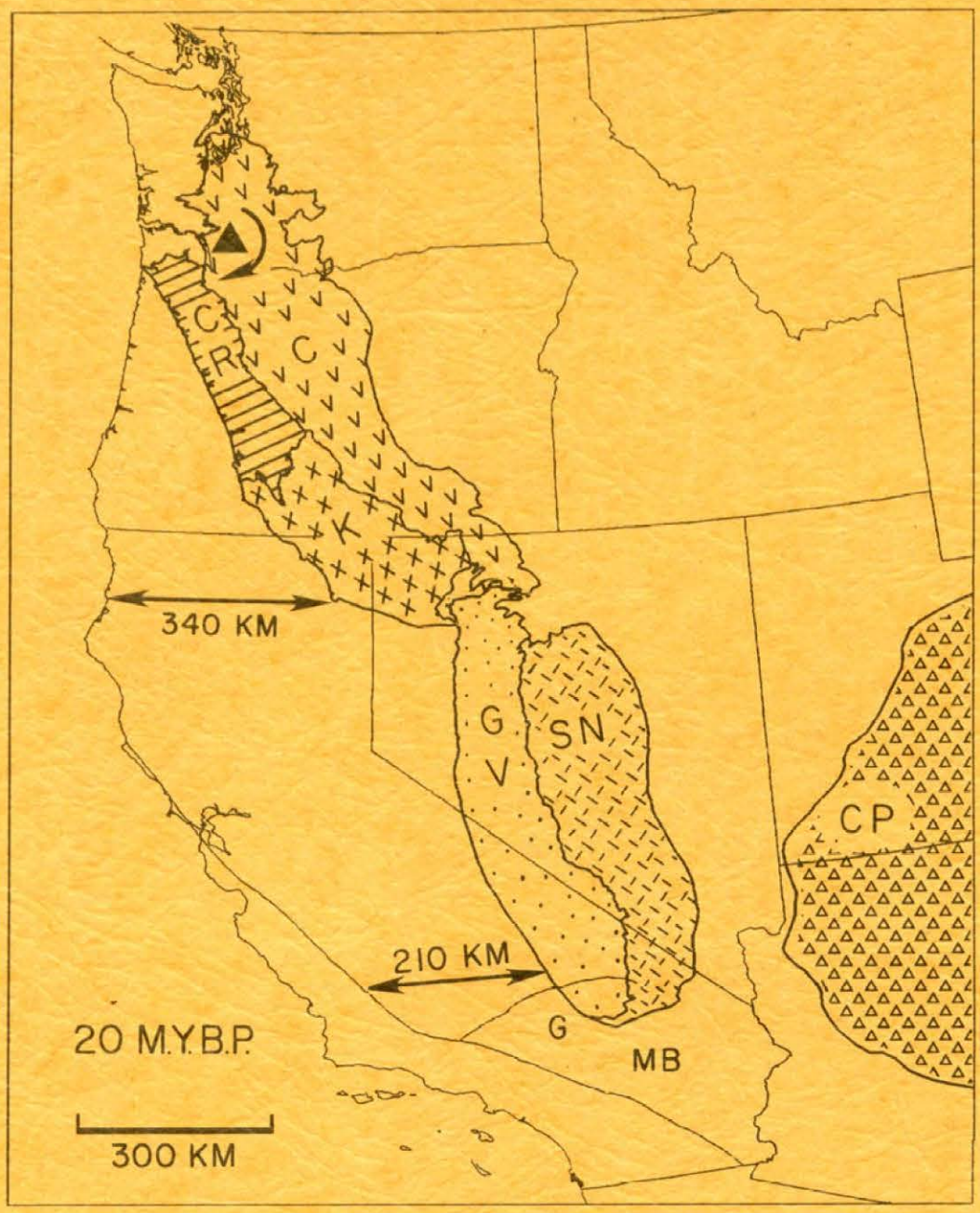

1980

STATE OF OREGON
DEPARTMENT OF GEOLOGY AND MINERAL INDUSTRIES
DONALD A. HULL, STATE GEOLOGIST

STATE OF OREGON
DEPARTMENT OF GEOLOGY AND MINERAL INDUSTRIES
1069 State Office Building, Portland, Oregon 97201

Special Paper 10

TECTONIC ROTATION OF THE OREGON WESTERN CASCADES

James Magill and Allan Cox
Department of Geophysics, Stanford University

1980

Conducted in conformance with ORS 516.030.
Funded in part under U.S. Department of Energy Contract
DE FC 07-79-ID-12044
to the Oregon Department of Geology and Mineral Industries

NOTICE

The Oregon Department of Geology and Mineral Industries is publishing this paper because the subject matter is consistent with the mission of the Department. To facilitate timely distribution of information, camera-ready copy submitted by the authors has not been edited by the staff of the Oregon Department of Geology and Mineral Industries.

CONTENTS

ILLUSTRATIONS

Figures:

ILLUSTRATIONS (cont.)

Figures:

Tables:

TECTONIC ROTATION OF THE OREGON WESTERN CASCADES

INTRODUCTION

Anomalous directions of magnetization in Tertiary rocks of the Coast Range of Oregon (Figure 1) (Simpson and Cox, 1977; Beck and Plumley, in press; Magill et al., in press) have established that Cenozoic sedimentary and volcanic rocks have undergone clockwise rotations about vertical axes of from 35^{0} to 75^{0} (Figure 2). Paleomagnetic sampling has been extensive in both the number of individual rock samples analyzed and the number of geologic units studied. The observation that similar clockwise rotations are recorded in rocks of varying Cenozoic age as petrologically dissimilar as basalts and turbidites leaves little doubt that the anomalous paleomagnetic directions have recorded a true tectonic rotation. The regional geology and consistency in the paleomagnetic data indicate that the Coast Range rotated as a single coherent block extending from the Klamath Mountains northward to the Oregon-Washington border. This coherence and the apparent absence of major cross-cutting tectonic boundaries are supported by several geologic observations: (1) the continuity of outcrop of middle Eocene Tyee and Flournoy formations along the entire Coast Range defining it as a single Eocene basin rather than a tectonic composite of several basins, (2) the absence of strong deformation in these formations, and (3) the internal consistency of current directions recorded in the turbidites of these formations throughout the Coast Range (Snavely et al., 1964). The structural continuity suggested by these observations is further supported by the presence of a pronounced gravity high (Bromery and Snavely, 1964) extending from the northern to the southern part of the Coast Range suggesting an elongate regional structure. The smooth gravity contours characteristic of the Coast Range do not display the offsets or short wavelength features that are commonly associated with major tectonic structures. The available geophysical and geologic data are thus consistent with the Oregon Coast Range having rotated as one quasi-rigid block extending from the Klamath Mountains to the Oregon-Washington border.

Concerning the geologic names used in this paper, we are aware that the stratigraphic correlations and formation names in western Oregon are currently undergoing extensive revision. To minimize confusion, we have used the names used by the authors we cite. The

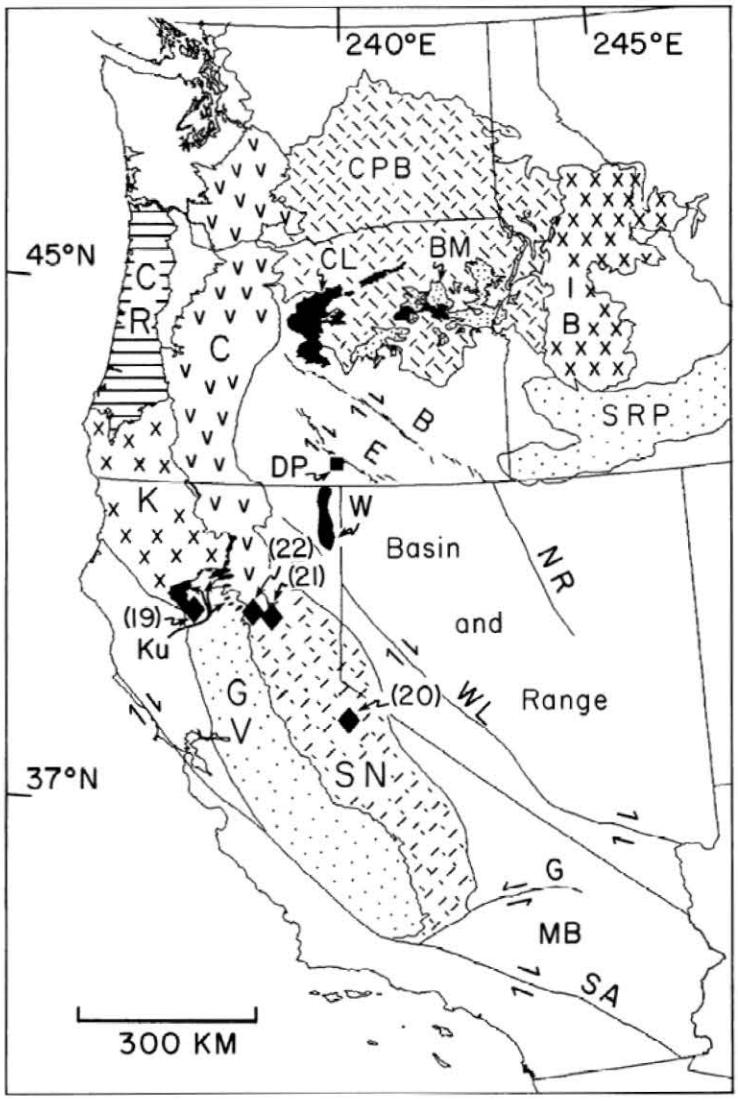

Figure 1. Generalized geotectonic map of the western U.S. based on Cohee (1962) and Lawrence (1976). C=Cascades, CR=Oregon Coast Range, CL=Clarno Formation, BM=Blue Mountains, CPB=Columbia Plateau Basalts, DP=Drake Peak, GV=Great Valley, IB=Idaho Batholith, K=Klamath Mountains, Ku=Upper Cretaceous sediments, MB=Mojave block, NR= Nevada rift, SN=Sierra Nevada, SRP=Snake River Plain, W=Warner Mountains. Fault Zones: B=Brothers, E=Eugene-Denio, G=Garlock, SA=San Andreas, WL=Walker Lane. The numbered locations refer to paleomagnetic sampling localities identified in Table 3.

discerning reader will recognize that some of these are no longer accepted and will make the necessary translation.

In attempting to incorporate the paleomagnetically observed rotation of the Oregon Coast Range into the geologic history of the region, it is important to know the regional extent of the rotated block, the timing of the rotation and a viable mechanism to produce the rotation.

Where are the boundaries of the rotated region ?

Several lines of evidence suggest that the coherent rotated Coast Range block extends north to the Washington border but not beyond. In contrast to the long wavelength anomaly over the Oregon Coast Range, gravity anomalies over the the Washington Coast Range are of short wavelength with sharp gradients suggestive of local crustal tectonic structures. Moreover, north of the Oregon-Washington border, paleomagnetic results from the Black Hills and Willapa Hills show variable rotation from region to region and indicate less rotation than that recorded in similar age rocks to the south (Globerman and Beck, 1979; Wells and Coe, 1979). The emerging picture is one of different amounts of rotation in different tectonic blocks north of the Columbia River contrasted with the coherent rotation of one block to the south.

In southern Oregon the predominately Cenozoic terrane of the Coast Range meets the mainly Mesozoic terrane of the Klamath Mountains (Figure 1) along a geologic boundary that may or may not be a Cenozoic tectonic boundary. The possibility that the Klamath terrane rotated with the Oregon Coast Range during the Cenozoic has not yet been tested paleomagnetically. To the east, the early Tertiary rocks of the Coast Range pass beneath the middle and late Tertiary and Quaternary volcanics and sediments of the Cascade arc. The question of whether the Cascades have participated in the rotation of the Coast Range is the subject of this paper and of much current research (Bates et al., 1979; Bates and Beck, in press; Beck and Burr, 1979).

When did the rotation occur ?

Did the rotation occur throughout the Cenozoic or was it completed by the Miocene or some earlier time? An important observation is that the post-Oligocene Coast Range rocks (Clark, 1969; Simpson and Cox, 1977; Beck and Plumley, in press) and basalts and andesites of the western Cascades of Washington (Bates et al., 1979; Bates and Beck, in press; Beck and Burr, 1979) are rotated significantly less than older Eocene rocks of the Oregon Coast Range (Simpson and Cox, 1977; Magill et al., in press) implying that significant rotation occurred before as well as after Oligocene time. Our paleomagnetic results from Oligo-Miocene Cascade rocks help to further establish and refine these constraints on the timing

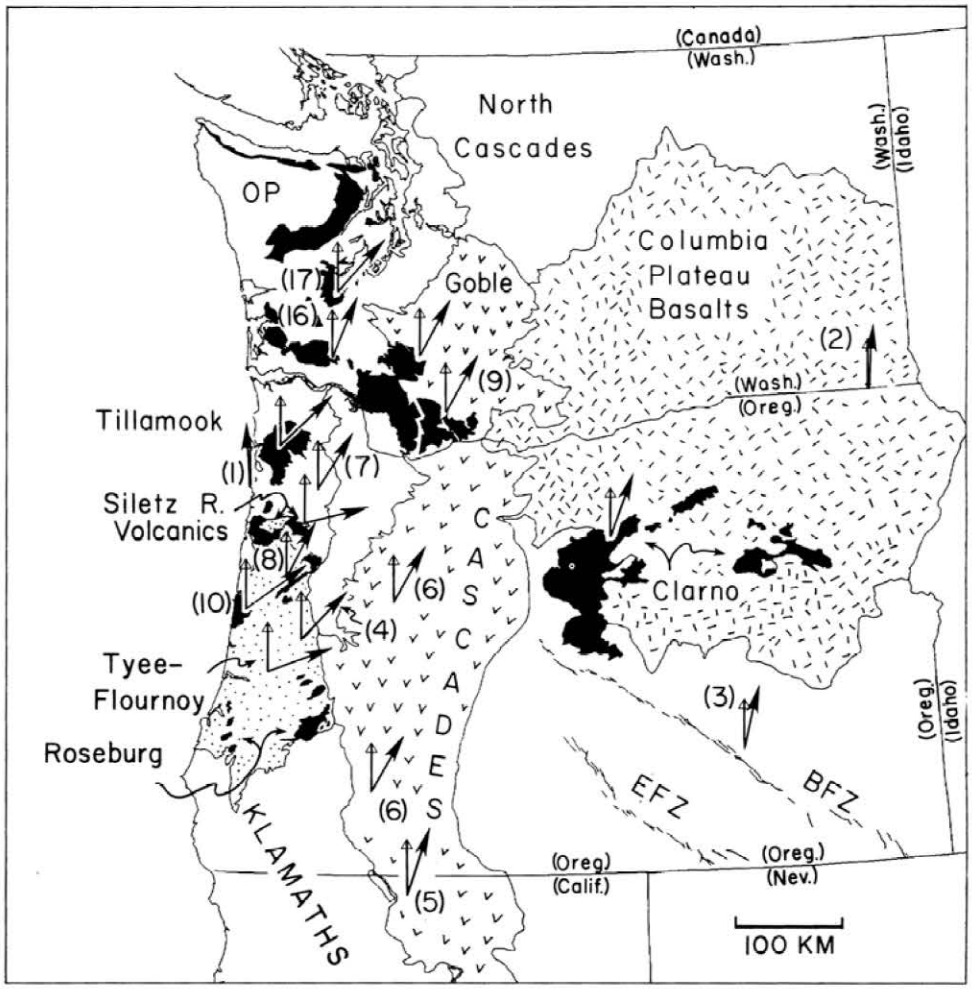

Figure 2. Generalized geotectonic map of Oregon and Washington. Arrows indicate the mean paleomagnetic directions found for the respective geologic units. The open arrow marks the expected declination and the solid arrow the observed declination. The arrows have been adjusted so that the expected declinations point due north. An easterly directed solid arrow therefore indicates a 90^{0} clockwise rotation. The arrows are labeled by geologic names or numbers listed in the rotation data summary of Table 3. Paleomagnetic results reported in this paper were collected in the Oregon Western Cascades at two localities labeled (6). A paleomagnetic direction for the Coast Range Eocene intrusions ((12), Table 3) and outcrops of the Miocene Intrusions (4), Oligocene Intrusions (7) and the Blue Mountains (Figure 1) are not shown for simplicity. Map is based on Huntting et al (1961), Wells and Peck (1961), Cohee (1962), Lawrence (1976) and Walker (1977).

and regional extent of the rotation.

By what mechanism did the rotation occur ?

The oldest rocks in the Coast Range (Figure 2), the lower and middle Eocene Siletz River Volcanics and the correlative lower Eocene Roseburg Formation, consist of tholeiitic pillow basalts, intercalated marine volcanic sediments and subaerial alkalic basalts (Snavely and Wagner, 1963; Snavely et al., 1968; Baldwin, 1974, 1975). The overlying middle Eocene Tyee-Flournoy formations are marine turbidite sandstones and siltstones (Snavely et al., 1964; Lovell, 1969; Baldwin, 1974). Flow structures and distinctive lithologies indicate that the main source of the middle Eocene sediments was to the south in the Klamath Mountains. Continued basaltic volcanism through the middle and late Eocene produced the Yachats basalt (Snavely and MacLeod, 1974) and the Tillamook Volcanic Series (Snavely et al., 1970; Beaulieu, 1971, Nelson and Shearer, 1969).

Information about the original tectonic setting of the rocks of the Coast Range is provided by geologic, geochemical, and geophysical data. The lower Eocene Coast Range basalts are marine and are overlain by lower, middle and upper Eocene basalts with major-element chemistry most similar to that of oceanic island provinces (Snavely et al., 1968; Glassely, 1974) like the present-day Hawaiian Islands. Trace-element data from the lower marine basalts (Loeschke, 1979) is supportive of formation as either an oceanic island or ocean ridge. The overlying basalts, the upper Siletz volcanics, the Yachats and the upper Tillamook basalts are all subaerial and therefore appear to cap an emergent island complex. Correlative (Eocene) pillow basalts to the north in the Olympic Peninsula (Baldwin, 1974; Cady, 1975) are associated with pelagic limestones (Garrison, 1973), consistent with an oceanic island setting. Snavely et al. (1968) have estimated the thickness of the Siletz basalts at 10,000 to 20,000 feet, clearly anomalously thick crust. This and an even greater crustal thickness of 15 to 20 km determined for the Coast Range from seismic data (Tatel and Tuve, 1955; Berg et al., 1966; Langston and Blum, 1977) are consistent with a basement of oceanic crust anomalously thick due to the presence of oceanic islands. This model for the Coast Range basement is supported by the regional geology, by regional isotopic data and by seismic, gravity and resistivity data as summarized by Simpson (1977). All appear to support the existence of oceanic crust beneath a large part of western Oregon and southwestern Washington (Hamilton, 1969, 1978; Dickinson, 1976; Davis et al., 1978) and suggest that the Eocene basalts that now form the Coast Range were a seamount province.

Considering the original oceanic setting for the Oregon Coast Range rocks, the paleomagnetically observed rotation would appear to be most easily related to accretion of the seamount province to North America. Evidence for an early Eocene collision of the seamount province with North America is found in the geology of the southern Oregon Coast Range. At the extreme southern end of the range, the presence of a subduction zone is

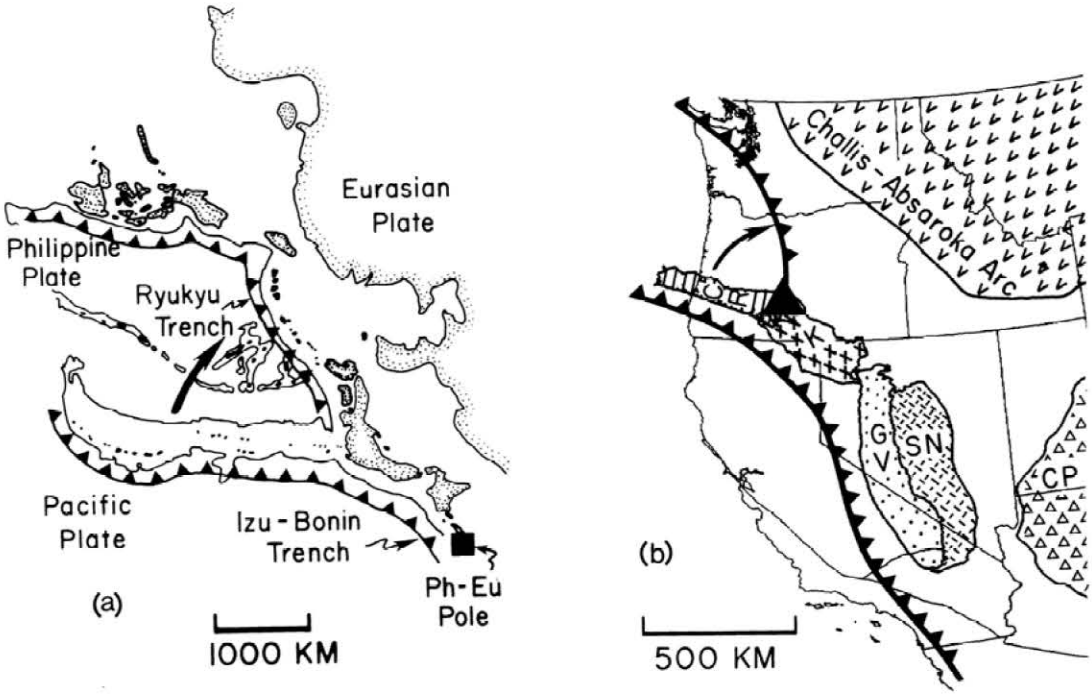

Figure 3. A comparison of Phase I rotation (b) with a modern-day analogue from the western Pacific (a). Reconstruction (b) shows the position of the proposed tectonic blocks at the beginning of Phase I rotation, 50 m.y.b.p. See Figure 1 for the present-day position of these blocks. The rotation pivot at the southern end of the Coast Range block is shown by a triangle. In (a) the Philippine plate and adjacent regions have been rotated to the Oregon-Washington area and plotted with the same map projection as (b) to minimize distortion. The Philippine-Eurasia relative motion pole of Seno (1977) is shown by a solid box (Ph-Eu).

recorded in the early Eocene Roseburg Formation (Baldwin, 1974, 1975). The latter includes submarine basalts and marine sediments that are intensely thrusted and isoclinally folded, with late Cretaceous sediments being folded into the Roseburg during an early Eocene episode of intense deformation. We interpret this deformation to mark a subduction zone. Beaulieu (1971, p.30) notes that the Roseburg (lower Umpqua) has several features of a melange. Strong northwestward vergence of the folds in the lower Eocene strata of southern Oregon is suggestive of underthrusting from the northwest (Baldwin, 1964). Some Roseburg strata were tectonically emplaced within the neighboring Jurassic Otter Point Formation of the Klamath terrane, and the Roseburg contains exotic blocks of schist and greenstone and conglomerate all derived from the Klamaths, so the subduction zone at the southern end of the Coast Range was located near shore in the early Eocene. Subduction at this locality stopped abruptly at or near the end of the lower Eocene. The gently folded middle Eocene turbidites and conglomerates of the Tyee and Flournoy formations which overlie the Roseburg formation with an angular unconformity display none of the thrusting and telescoping of strata that characterized the underlying Roseburg Formation. The simplest explanation is a westward jump of the subduction zone toward the end of the lower Eocene.

Magill et al. (in press) have recently proposed that collision of the Coast Range seamount province began the first phase of a two-phase rotation of the Coast Range. During Phase I (Figure 3), the Coast Range underwent clockwise rotation when it became trapped between two active trenches. Rotation (46^{o}) and continued volcanism in the Coast Range occurred as the wedge-shaped plate was consumed in the eastern trench. The pivot point was near the present location of the Roseburg Formation, the volcanics and sediments of which jammed the trench at its southern end. By the end of the Eocene the subduction zone to the east was no longer active and the marine oceanic rocks of the Oregon Coast Range had become part of the North American plate. A modern analogue of the proposed rotation and subduction zone geometry would be the piece of sea floor (Philippine plate) bounded by the active Ryukyu and Izu-Bonin trenches in the western Pacific. Present-day motion of the Philippine plate relative to Eurasia (Seno, 1977) indicates that the Philippine plate is rotating clockwise into the Ryukyu trench about a local pivot (Figure 3) similar to the proposed Eocene rotation of the Oregon Coast Range.

Phase II of the Oregon Coast Range rotation accounting for a further 30^{o} of rotation is suggested to be a late Cenozoic event related to extension in the Basin and Range province. We will return to this model later in the paper.

WESTERN CASCADES

Geology and paleomagnetic data

The Cascade Range extends nearly due north from northern California into British Columbia. In Oregon the range has a length of nearly 400 km and a width of 50 to 120 km and lies directly east of the Coast Range and Klamath Mountains. The Pliocene and Quaternary shield volcanos, stratovolcanos and cinder cones of the High Cascades are underlain by late Eocene to Miocene basalts, basaltic andesite, andesite flows and pyroclastics (Peck et al., 1964; Wise, 1969). Rocks from this earlier episode of volcanism are termed the Western Cascades and outcrop primarily on the western side of the High Cascades. The combination of age and geographic position east of the Coast Range and Klamaths make the Oregon Western Cascades of particular interest for paleomagnetic study. If the Cascades have rotated with the Coast Range we would expect to find the greatest amount of rotation in the Western Cascades since they are the oldest units within the Cascades. In addition, their position directly east of the Coast Range block and the existence of depositional contacts linking the Cascades to the Coast Range and Klamaths (see discussion below) permit the extrapolation of results from the Cascades to the Coast Range and Klamaths, thereby increasing the geographic and temporal constraints on rotation of the Coast Range and continental margin.

Paleomagnetic samples were collected from two regions in the Western Cascades of Oregon 200 kilometers apart (Figure 2, sites 6), the northern one in the Sweet Home quadrangle and the southern one in the Butte Falls quadrangle. The geology of the northern sampled section consists of subaerial flows of basalt and basaltic andesite of the Little Butte and Sardine formations as mapped by Peck et al. (1964) (Figures 4,5 and 6). Geochemical and age data show these rocks to be similar to typical island arc tholeiites (except for anomalously high Th, U, and Rb and enriched REE patterns) and to range in age from 20 to 30 m.y. (White and McBirney, 1979). Most of our paleomagnetic samples were taken from the same flows sampled by White and McBirney to assure good age control. The regional structure is relatively uncomplicated and has not been affected by any significant faulting. Regional tilts in the 700 meters of sampled section are less than 5^{o} and appear randomly oriented. Such tilts likely reflect the original dip of the lava flows.

The southern sampled section (Figure 7) has been mapped by Wilkinson et al. (1941) and J. Smith of the U.S.G.S. (personal communication) as consisting of subaerial flows of basalt and basaltic andesite of the Roxy and Wasson formations within the Little Butte volcanics. The 3000 meters of sampled section is of latest Oligocene age based on K-Ar dating by J. Smith (personal communication). Again the regional structure is uncomplicat-

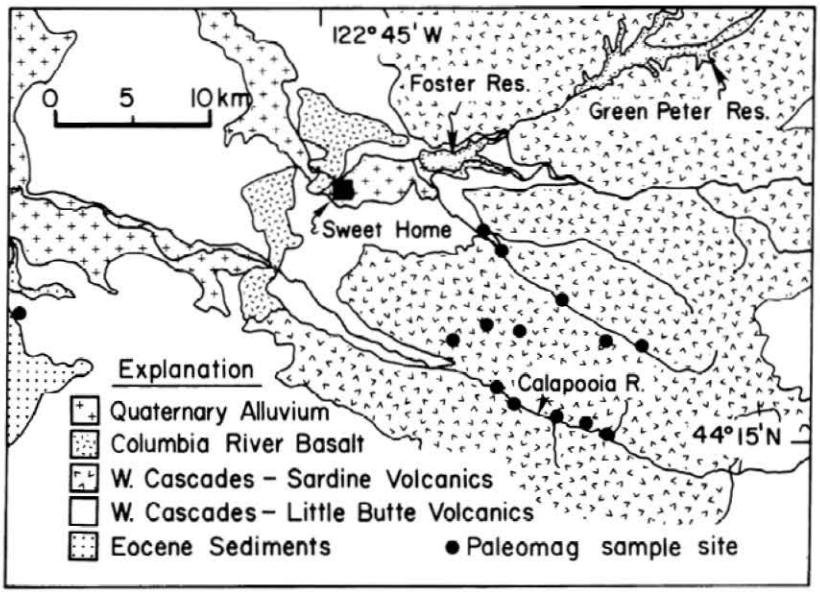

Figure 4. Generalized geologic map of the northern paleomagnetic sampling locality in the Western Cascades. Geologic boundaries and stratigraphy are from Peck et al. (1964). Note the onlapping contact of the Western Cascade rocks upon the Eocene sediments of the Coast Range.

Figure 5. Typical outcrop within the Western Cascades. Outcrop shown lies just northwest of paleomagnetic site S034 along the Calapooia R. in the northern sampling locality (SW 1/4 Sec. 6, T. 15 S., R. 2 E., Sweet Home quadrangle).

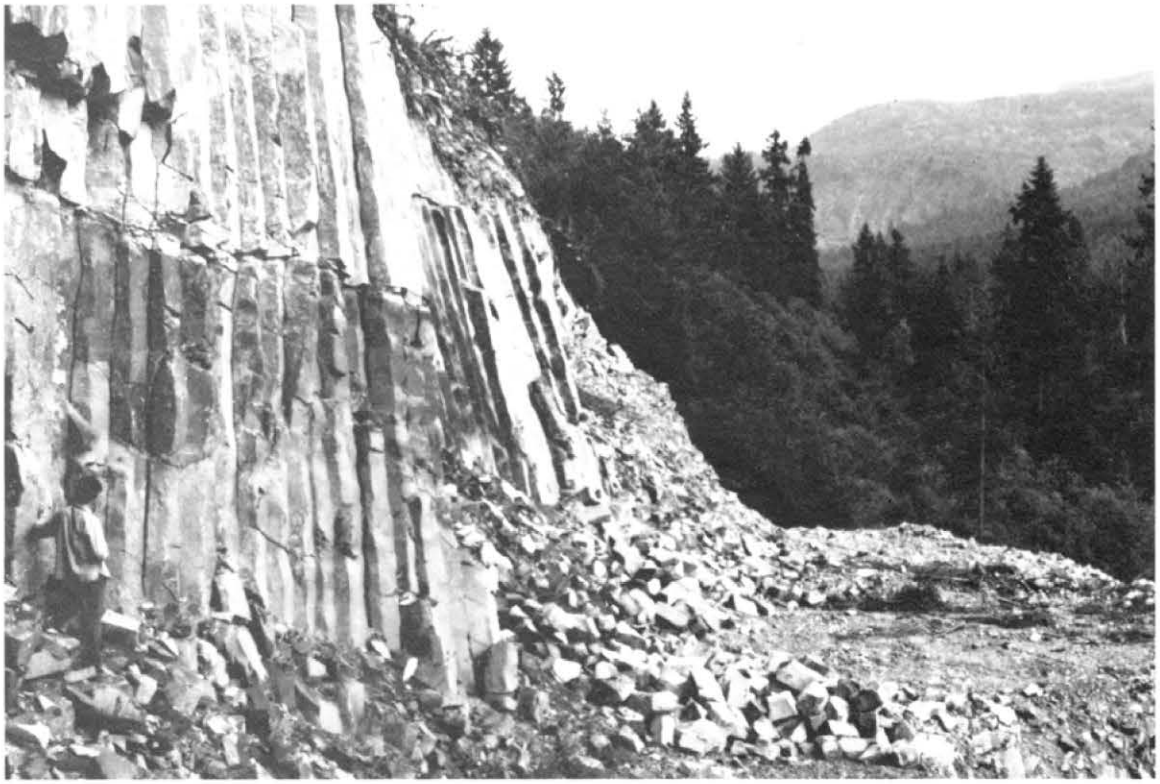

Figure 6. Columnar jointed flow or sill in the northern sampling locality located along Wiley Creek (SE 1/4 Sec. 7, T. 14 S., R. 2 E., Sweet Home quadrangle). Paleomagnetic samples of site S066 were collected from this flow or sill.

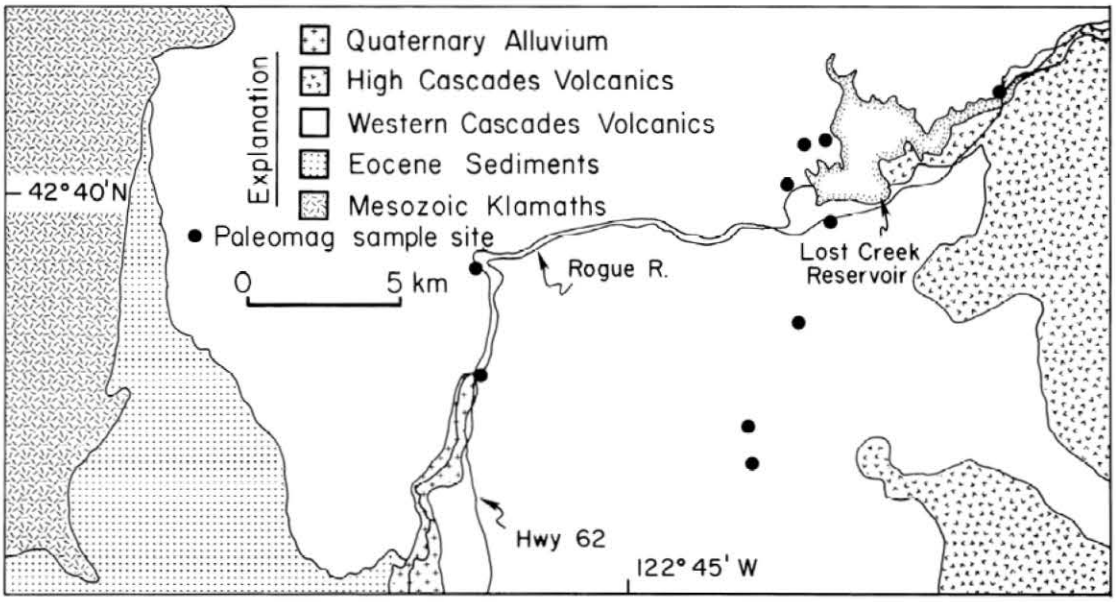

Figure 7. Generalized geologic map of the southern paleomagnetic sampling locality in the Western Cascades. Geologic boundaries and stratigraphy are from Wilkinson et al. (1941). Note the onlapping contact of Western Cascade rocks upon Eocene and Mesozoic Klamath terrane.

ed, detailed mapping showing no faults with significant displacement (J. Smith, personal communication). The regional structure has a uniform tilt of 7^{o} to the northeast.

From 5 to 8 samples were collected from each of 17 sites in the northern locality and 11 sites in the southern locality. Each site consists of samples from a single lava flow or dike and therefore represents a single instantaneous measurement of the paleomagnetic field. Individual samples were drilled at the outcrop with a portable diamond drill and oriented with a magnetic compass prior to removal from the outcrop, taking care to compensate for local magnetic anomalies using backsiting techniques. All samples were stepwise magnetically cleaned in alternating peak fields ranging from 5 to 100 milliteslas (see Appendix for data listing). The directional stability and coercivity spectrum of each sample was used to determine the optimum field for cleaning. Figures 8 and 9 show typical examples of our data plotted on Zijderveld component plots. After removal of a secondary overprint at low demagnetization fields, most samples experienced the removal of only a single component of magnetization during further demagnetization. The straight demagnetization trends which intersect the origin as in Figures 8b and 9a show the removal of a

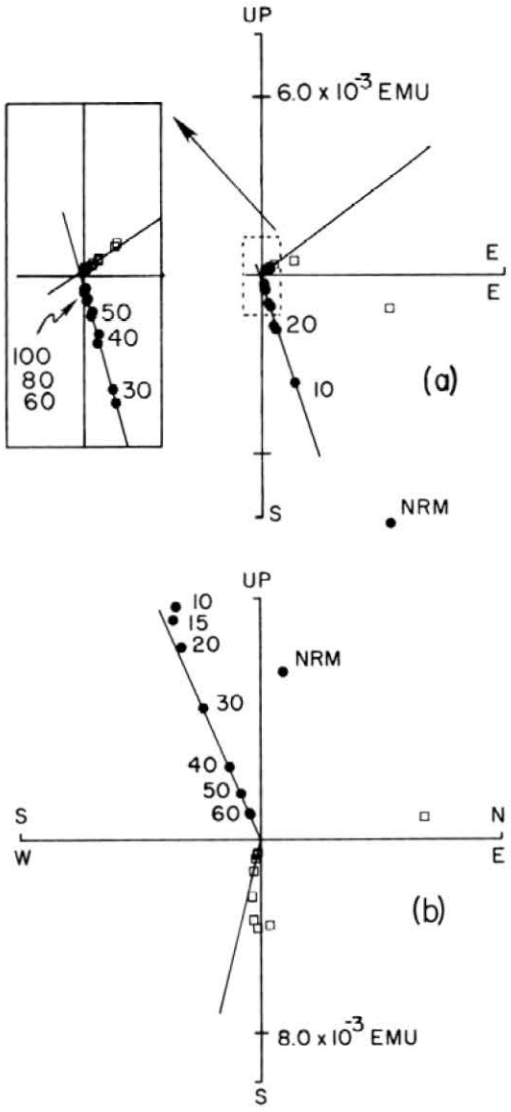

Figure 8. Zijderveld component plots for samples (a) S034-1 and (b) S072-1 during stepwise alternating field demagnetization. The open boxes represent the north and east components (a,b) and the dots the down and east (a) and up and north (b) components. The demagnetization field values are shown in milliteslas.

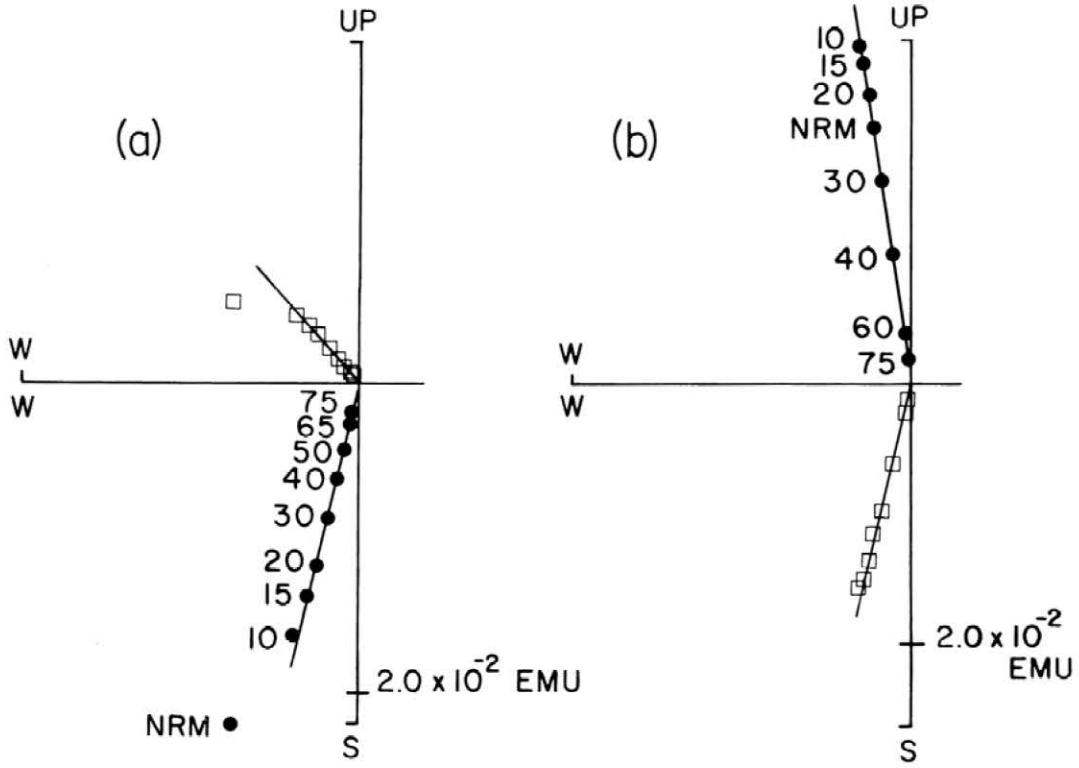

Figure 9. Zijderveld component plots for samples (a) L034-1 and (b) L053-1 during stepwise alternating field demagnetization. The open boxes represent the north and west components and the dots the up and west components. The demagnetization field values are shown in milliteslas.

Table 1. Summary of paleomagnetic data from the Western Cascades

Site	*Declination*	*Inclination*	α_{95}	κ	*N*	*H*
Northern sites:						
S001	57.9	63.3	4.6	174	7	20-70
S008	207.4	-46.8	5.8	110	7	30-70
S015	196.6	-49.1	3.9	243	7	20-60
S022	209.4	-63.0	6.5	139	5	20-80
S028	357.4	75.6	11.8	33	6	20-30
S034	40.4	72.2	5.0	231	5	20-40
S046	193.3	-57.7	4.4	234	6	20-80
S052	58.3	76.0	2.0	1084	6	30-40
S058	266.1	79.4	7.9	50	8	20-70
S066	53.9	79.0	3.6	357	6	10-15
S072	185.2	-65.3	5.2	136	7	20-40
S085	138.9	-86.8	3.3	341	7	10-70
S092	92.3	-88.3	3.2	451	6	20-60
S104	356.0	62.1	5.7	114	7	10-50
Southern sites:						
L001	22.3	61.9	4.7	169	7	10-30
L014	25.3	28.5	5.9	167	5	10-80
L028	17.2	64.4	2.6	646	6	20-40
L034	337.1	70.7	3.3	337	6	10-30
L040	99.0	67.1	9.0	46	7	10-50
L053	204.4	-60.4	3.1	377	7	15-40
L060	68.6	-71.8	6.8	128	5	20-60
L066	23.7	54.7	3.0	497	6	10-30
L072	45.6	55.4	8.7	60	6	15-40
L078	351.8	62.9	3.2	358	7	10-40

α_{95} = radius of 95% confidence in degrees, κ = precision parameter, N = number of samples, H = range of demagnetization cleaning fields in milliteslas which were used to determine (by single measurement or vector subtraction techniques) the directions of remanent magnetization of the N samples.

single component. In a few cases the demagnetization trends were straight but did not intersect the origin, e.g. Figures 8a and 9b. This behavior was interpreted to be the result of the superposition of the primary magnetization with a small secondary magnetic overprint, likely a chemical alteration. This interpretation is supported by the extremely hard magnetization of the overprint, magnetic cleaning having little or no effect on its intensity. The hardness of this magnetization is clearly seen in the demagnetization trends of Figures 8a and 9b since the trends are straight, not curved as would be the case for the simultaneous removal of two magnetic components. The primary magnetization was recovered from samples similar to L053-1 for Figure 9b by analysis of the magnetic vectors removed during demagnetization, this being a standard laboratory technique. Rocks from four sites (three from the northern and one from the southern locality) were found to be magnetically unstable or overprinted by secondary magnetizations and were not included in our final synthesis. The remaining sites were of high magnetic quality with 9 of reversed polarity and 15 of normal polarity. Circles of 95% confidence were usually about 4° and in all cases less than 12° (Table 1). The general existence of only a single component during cleaning, the magnetic stability of this component, and the existence of nearly antipolar reversals lends confidence to the conclusion that the primary remanent magnetization has been recovered. Figure 10 shows a summary of the site mean directions after magnetic cleaning and correction for regional tilt of sites from the southern locality. The measured field directions clearly show a significant clockwise rotation from the expected Oligo-Miocene field direction for stable North America. Accounting for dispersion in the measured and expected field direction, the clockwise rotation is found to be $25^{\circ} \pm 20^{\circ}$ with 95% confidence (Table 2).

TABLE 2. Paleomagnetic results -- Western Cascades

	Pole					Field Direction		Flattening		Rotation	
	N Lat	E Long	α_{95}	N	κ	Inc.	Dec.	F	ΔF	R	ΔR
Observed	72.2	280.0	10.9	24	8.3	70.1	20.7	-8.0	8.1	24.7	19.7
Expected	87.0	162.0	4.0	21	66.0	62.1	356.0				

Explanation: Expected field from Irving (1979) for 25 m.y.b.p.

α_{95} = radius of 95% confidence about the mean pole, N=number of sites, κ=precision parameter, Inc. = Inclination, Dec. = Declination, $F = \text{Inc.}_{\text{expected}} - \text{Inc.}_{\text{observed}}$, $\Delta F = [\Delta I^2_{obs} + \Delta I^2_{exp}]^{\frac{1}{2}}$ where $\Delta I = 2\alpha_{95}/1 + 3\cos^2 p$, $R = \text{Dec.}_{\text{observed}} - \text{Dec.}_{\text{expected}}$, $\Delta R = [\Delta D^2_{obs} + \Delta D^2_{exp}]^{\frac{1}{2}}$ where $\Delta D = \sin^{-1}[\sin\alpha_{95}/\sin p]$, p = colatitude.

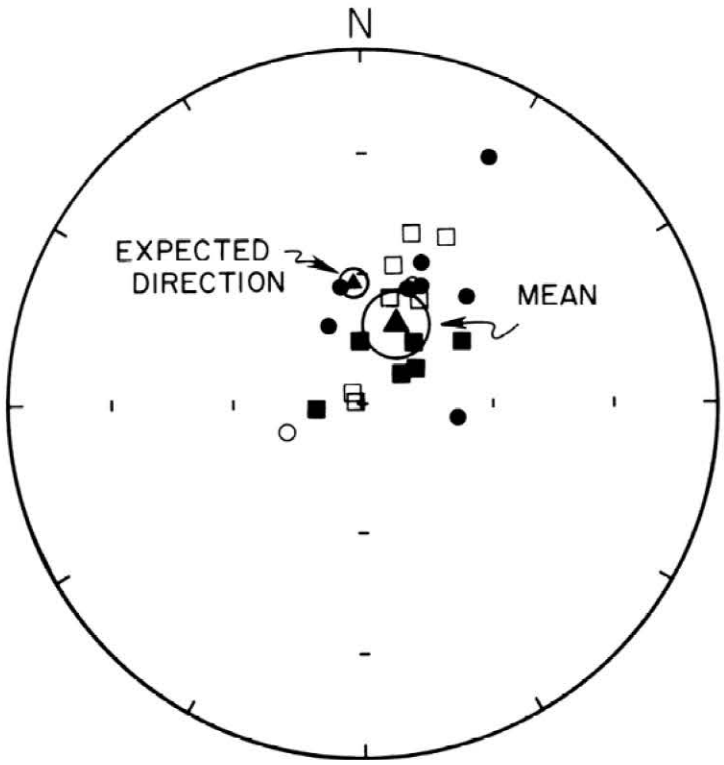

Figure 10. Paleomagnetic field directions for sites from the Oregon Western Cascades (Table 1), northern locality average site directions are shown by boxes and southern locality directions (corrected for tectonic tilt) by circles. Directions of normal polarity are plotted as filled symbols and those of reversed polarity as open symbols. Directions of reversed polarity have been reflected through the origin to plot on the lower hemisphere of this stereo polar plot. The mean direction was computed from the mean pole of the 24 site VGP's. The circles about the expected and observed means (Table 2) are the 95% confidence circles (α_{95}).

The mean measured inclination (70^{o}) and the expected inclination (62^{o}) differ by $8^{o} \pm 8.1^{o}$ with 95% confidence (Table 2). If this difference is real, one possible explanation of the steep inclination is that the Western Cascade volcanics underwent a southward translation of 1200 km since emplacement, but this is ruled out by the depositonal contact (see below) linking the Western Cascades and the Coast Range. Paleomagnetic data from the Coast Range do not have steep inclinations and therefore do not indicate southward translation. A more likely explanation of the steep inclination is that the strata may have undergone a regional tilt of about 5^{o} or so eastward toward the north-trending subsiding axis of the Cascade Range (Peck et al., 1964). The strata are nearly horizontal today because they were initially deposited with a dip of 5^{o} or so to the west, which is reasonable since all the known Oligo-Miocene vents of the Western Cascade volcanics lie some 40 to 50 km east of each of the sampling localities (Peck et al., 1964). It is important to note that a hypothetical westerly tilt bringing the measured and expected inclinations into agreement increases the implied rotation to about 28^{o}. We therefore consider the measured mean rotation of the Western Cascades of 25^{o} to be a minimum.

Regional interpretation

Our new paleomagnetic data from the Western Cascades, when combined with three other Cascade paleomagnetic studies, strongly suggests a uniform rotation of the Cascade Range from northern California to central Washington. Paleomagnetic results from basalts and andesites of the early Cascade Goble Volcanics (32 to 45 m.y.) and Ohanapecosh Formation (31 to 37 m.y.) of southern Washington (Figure 2) show rotations of $28^{o} \pm 12^{o}$ (Beck and Burr, 1979) and $35^{o} \pm 12^{o}$ (Bates and Beck, in press) respectively. Moreover, a reinterpretation of the paleomagnetic study of Beck (1962) of Western Cascade rocks (latest Eocene to Miocene) in northern California (Figure 2) indicates $18^{o} \pm 14^{o}$ clockwise rotation. In this early study Beck (1962) interpreted the clockwise-rotated magnetization directions as the result of improper statistical sampling or anomalous behavior of the geomagnetic field. Considered in the context of the present results from Cascade rocks of similar age, Beck's results from the Cascade rocks in northern California appear to have recorded a true tectonic rotation. These three studies combined with our results yield an average clockwise rotation (weighted by 95% confidence limits) of $27^{o} \pm 7^{o}$. The internal consistency is remarkable and is clearly indicative of a tectonic rotation affecting a broad region including the entire Western Cascades and adjacent terrane.

Having established the tectonic rotation recorded in rocks of the Western Cascades, the geologic contacts of the Cascades with the adjoining Coast Range and Klamaths to the west take on considerable significance. These geologic contacts are predominantly depositional contacts rather than fault contacts. This relationship is observable in south-central Oregon and northern California where basal Cascade rocks (Colestin and Spencer Fm.) lie conformably and unconformably on early and middle Eocene Coast Range rocks

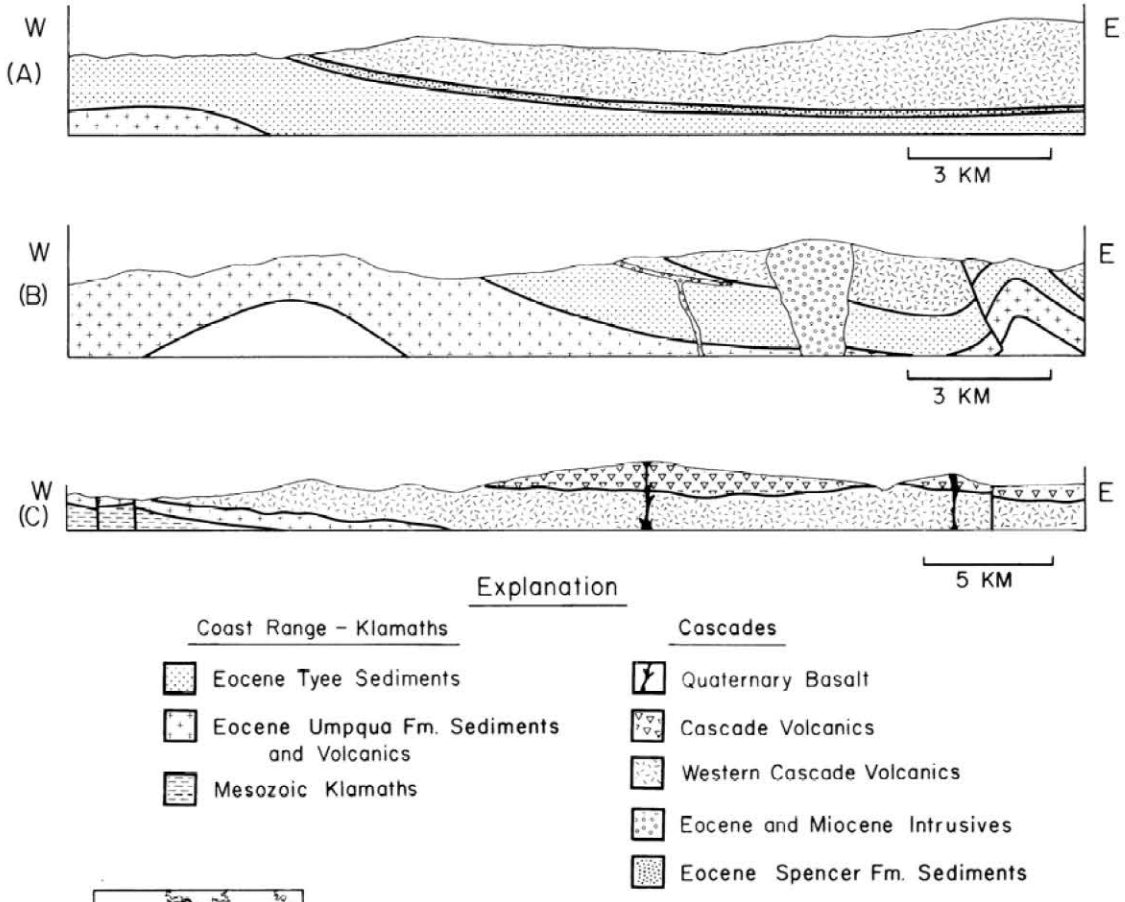

Figure 11. Geologic cross sections showing the onlapping relationship of Cascade rocks upon the rocks of the Coast Range and Klamaths. The location of the cross sections are shown in the inset. Sections are shown without vertical exaggeration. Sources for the cross sections and stratigraphy are: (A),(B) Hoover (1963); (C) Williams (1949).

(Umpqua and Tyee) (Figure 11) (Wilkinson et al., 1941; Hoover, 1963) and pre-Tertiary rocks of the Klamath Mountains (Wilkinson et al., 1941; Wells and Peck, 1961) (Figure 11). Similar depositional contacts between the Cascades and Coast Range exist in southern Washington (Snavely et al., 1958; Roberts, 1958; Hammond, 1979). These onlapping relationships and similar depositional relationships of the paleomagnetically sampled units upon the basal formations of the Cascades require that both the Coast Range and Klamaths participated in the 25° post-25-m.y.b.p. rotation of the Cascades. This collective rotation of the Cascades, Coast Range and Klamaths amounts to rotation of a large segment of the continental margin of western North America and places significant constraints on Oligocene paleogeographic reconstructions.

A significant implication of the post-25-m.y.b.p. rotation of the Cascades, Coast Range and Klamaths is that this rotation must have resulted from internal deformation of the North American continent. Since the Cascades are arc volcanic products of subduction west of the Coast Range, the convergent margin must have lain some 150 to 200 km west of the Cascades. This inland position of the Cascade Range together with its position east of the Mesozoic Klamath terrane eliminates the possibility that the rotation of the Cascades was associated with accretionary processes along a late Tertiary convergent margin. Rotation of the Cascades and Klamaths therefore appears not directly related to subduction and more likely is the result of broad internal deformation within the western Cordillera.

PALEOGEOGRAPHIC RECONSTRUCTIONS

Magill et al. (in press) have recently proposed that the regional geology and the paleomagnetic data can best be explained by a model with two distinct episodes of rotation, one during the middle Eocene (approx. 45°) and another between the Miocene and present (approx. 30°). Our results from the Cascades together with the onlapping nature of the contact of the Cascades with the Coast Range and the Klamaths support such a two-phase rotation model. Our results require that the Coast Range rotated with the Cascades about 25° clockwise during the past 25 m.y. The fact that early and middle Eocene rocks of the Coast Range are rotated as much as 77° (Table 3) leaves about 50° of Coast Range rotation unaccounted for by the rotation of the past 25 m.y. (Figure 12). This difference is too large to be due to experimental errors and indicates that the Coast Range block underwent an earlier phase of rotation. It is our interpretation that this earlier rotation occurred as a distinct episode during the middle and late Eocene and was followed by a period of tectonic stability during the Oligocene. To the eye, however, it might appear that the rotation and age data in Figure 12 could be fit by a simple straight line corresponding to rotation at a constant rate. To test statistically whether the data are simply linear we fit the paleomagnetic rotation and age data from the Cascades and Oregon Coast Range (Figure 12) with first, second, and third order polynomials, weighting the data by the 95% confidence limits of the respective rotations. Using an F test of the chi square statistics, the third order polynomial (inset of Figure 12) fits the data significantly better than a linear (95% confidence) or second order curve (50% confidence). This analysis does not prove that the third order polynomial fit is correct, but it indicates that the best fit curve is more complicated than a simple linear trend corresponding to rotation at a constant rate. The heavy curve in the inset of Figure 12 incorporates the basic shape of the fitted third order polynomial, modified a little to fit our interpretation of the regional geology (Magill et al., in press). The chi square of the interpreted heavy curve is slightly less than the best fit third order curve and therefore must be considered an equally good fit to the data. The Cascade results are clearly consistent with such a two-phase rotation.

The two-phase rotation curve of Figure 12 clearly shows that the rotation of the Goble Volcanics is consistent with the Goble being a member of the Coast Range-Cascade block and not a member of some separate block. Beck and Burr (1979) suggested that the Goble rotation (28°) is significantly smaller than the rotation of older rocks from the Coast Range and therefore the Goble is not part of the Coast Range block. We reject the separate block hypothesis for two reasons: (1) The Goble rotation is not statistically different at the 95% confidence level from the Coast Range Tillamook volcanics (Magill et

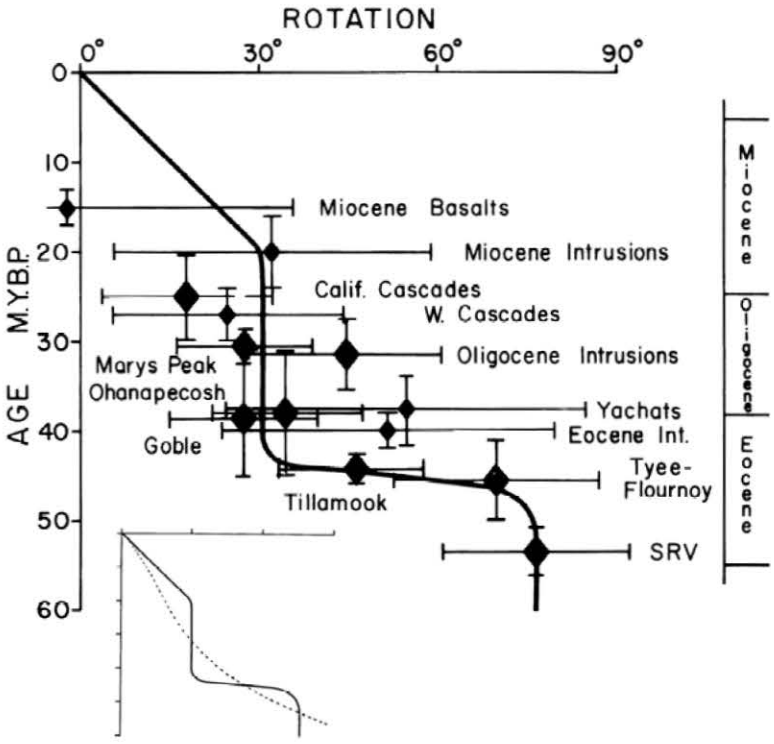

Figure 12. Rotation versus age for geologic units of the Cascades and Oregon Coast Range (Table 3). The rotation error bars are the ΔR values listed in Table 3. The inset shows a weighted least-squares fit of the data to a third order polynomial (dotted curve) contrasted with our suggested curve (solid) which is constrained by our interpretation of the regional geology.

Table 3: Compilation of regional paleomagnetic results from Oregon, Washington and the Sierra Nevada regions

Name and Reference		Observed Data: Pole Lat.	Pole Lon.	Pole α95	Pole N	Pole κ	Field Direction Inc.	Field Direction Dec.	Expected Field Age	Expected Field Inc.	Expected Field Dec.	Flattening F	Flattening ΔF	Rotation R	Rotation ΔR
Oregon-Washington Region															
Miocene Basalts	(1)	77.0	80.0	29.0	8	4.6	52.0	354.0	20	63.8	356.0	11.8	31.3	-2.0	35.8
Columbia R. Basalt N	(2)	87.6	203.2	7.0	6	91.6	65.7	357.7	20	64.8	355.8	-0.9	6.6	1.9	12.8
Columbia R. Basalt S	(3)	84.2	315.8	5.9	14	45.9	62.8	7.8	20	62.4	356.0	-0.4	6.3	11.8	10.8
Miocene Intrusions	(4)	----	----	9.6*	8	----	67.5	29.5	20	63.5	357.5	-4.0	----	32.0	26.8
California Cascades	(5)	78.7	292.9	8.9	24	12.0	65.5	13.8	25	61.5	356.0	-4.0	7.6	17.8	14.4
Western Cascades	(6)	72.2	280.0	10.9	24	8.3	70.1	20.7	25	62.1	356.0	-8.0	8.1	24.7	19.7
Oligocene Intrusions	(7)	----	----	8.4*	14	----	56.0	39.0	30	63.5	354.5	7.5	----	44.5	16.7
Marys Peak	(8)	63.0	8.0	8.0	26	13.5	42.0	22.0	30	64.0	354.6	22.0	11.3	27.4	11.4
Ohanapecosh	(9)	71.3	320.7	4.4*	34	----	63.6	26.8	35	65.3	352.2	1.7	----	34.6	12.4
Yachats Basalt	(10)	58.0	308.0	20.0	8	8.6	64.0	46.0	40	64.4	350.3	0.4	16.3	54.7	30.2
Goble Volcanics	(11)	75.5	345.5	5.5	37	17.7	57.5	18.5	40	65.4	350.1	7.9	6.4	28.4	12.4
Eocene Intrusions	(12)	----	----	12.5*	10	----	62.0	44.5	40	64.5	353.0	2.5	----	51.5	28.4
Clarno Formation	(13)	80.5	274.0	11.3	13	14.4	67.5	9.5	45	65.0	349.1	2.5	9.0	20.4	19.4
Tillamook	(14)	65.5	312.7	7.0	32	14.0	64.2	35.5	45	66.2	349.1	2.0	6.7	46.4	12.7
Tyee-Flournoy	(15)	49.0	305.0	11.0	40	5.2	63.0	59.0	45	65.3	349.3	2.3	9.6	69.7	17.2
Willipa Hills	(16)	----	----	----	--	----	----	10.0	50	67.6	347.8	----	----	22.2	----
Black Hills	(17)	69.4	322.3	5.2*	35	----	63.2	29.6	50	67.9	347.6	4.5	----	42.0	14.0
Siletz River Volc.	(18)	45.0	307.0	8.0	33	10.7	61.0	63.0	55	67.4	346.2	6.4	8.4	76.8	15.7
Sierra Nevada Region															
Great Valley	(19)	72.0	181.0	5.4	17	44.0	65.7	337.4	70	67.6	339.0	1.9	6.5	-1.6	13.7
Cretaceous Granites	(20)	68.8	195.2	9.6	14	18.0	68.1	336.0	85	67.0	333.6	-1.1	8.9	2.4	19.9
Bucks Batholith	(21)	57.6	194.8	7.9	9	43.7	72.1	317.1	140	60.4	333.6	-11.7	12.4	-16.5	22.9
Reeve Formation	(22)	73.0	139.0	9.0*	40	----	54.8	339.3	150	53.9	341.1	-0.9	----	-1.8	17.3

α_{95} = radius of 95% confidence about the mean pole, an (*) denotes an α_{95} of the mean field direction where the mean pole α_{95} was not available, N = number of sites, κ = precision parameter, Inc. = inclination, Dec. = declination, Age = age of the pole of Irving (1979) used to compute the expected field direction, $F = Inc._{expected} - Inc._{observed}$, $\Delta F = [\Delta I^2_{obs} + \Delta I^2_{exp}]^{\frac{1}{2}}$ where $\Delta I = 2\alpha_{95}/1 + 3\cos^2 p$, $R = Dec._{observed} - Dec._{expected}$, $\Delta R = [\Delta D^2_{obs} + \Delta D^2_{exp}]^{\frac{1}{2}}$ where $\Delta D = \sin^{-1}[\sin\alpha_{95}/\sin p]$, p = colatitude, or $\Delta D = \sin^{-1}[\sin\alpha_{95}/\cos(Inc.)]$ if an α_{95} for the mean field direction is only available. The Columbia R. Basalt N data is an average of sites SRC, LC, A, GR, M and I of Watkins and Baski (1974), Columbia R. Basalt S data is an average of sites BC, CC, PG, OR, S of Watkins and Baski (1974) and C, D1, D2, E, F, G, H, I of Watkins (1965). Other references are (1), (10), (15), (18) Simpson and Cox (1977); (4), (7) (12) Beck and Plumley (in press); (5) Beck (1962); (6) this study; (8) Clark (1969); (9) Bates and Beck (in press); (11) Beck and Burr (1979); (13) Beck et al. (1978); (14) Magill et al. (in press); (16) Wells and Coe (1979); (17) Globerman and Beck (1979); (19) Mankinen (1978); (20) Grommé and Merrill (1965); (21) Grommé et al. (1967); (22) Hannah and Verosub (1979).

al., in press), which are about 6 m.y. older than the Goble, and (2) 40 m.y. and younger rocks from the Coast Range and Cascades have an average rotation of 30°, in excellent agreement with the Goble rotation. This comparison to similar and younger age rocks is more appropriate than a comparison to older rocks for which the geology suggests an earlier accretionary rotation (Phase 1). It is our conclusion that the Goble rotation is anomalous only when compared to the oldest Coast Range rocks (Tyee-Flournoy, Siletz River Volcanic Series) and that this merely reflects the fact that the Coast Range was rotating during the middle Eocene (Phase I).

Considering the oceanic origin of the Coast Range seamount province and the volcanic arc origin of the Cascades, two distinct rotation phases seem reasonable because (1) the Coast Range and Cascades are two fundamentally different tectonic terranes, and (2) there is a significant difference in the maximum observed rotations for the Coast Range (77°) and Cascades (35°). We refer the reader to Magill et al. (in press) for more of the relevant geologic details of Phase I. Phase II of the rotation associated with extension of the Basin and Range province is of particular interest because it appears to be a viable model to explain the timing and magnitude of the Cascade rotation.

In Phase II rotation (Figure 13), the Coast Range, Klamaths, Cascades and northern end of the the Sierra Nevada all move westward in response to extension in the Basin and Range immediately to the east. The model explains the rotation as a consequence of the internal deformation of the continent and rotates the Coast Range, Cascades, and Klamaths together as one block as is required by the depositional geologic contacts. During Phase II, rotation of the Coast Range, Cascades, and Klamaths took place about a northern pivot and hence implies that extensional rifting was greater in southern Oregon than northern Oregon. Three observations suggest that this was the case. First, the distribution of late Cenozoic extensional faults delineating the Basin and Range province (Figure 14) suggests that extensional minima exist in northern Oregon and south of the Sierra Nevada, with a maximum at the latitude of the Oregon-Nevada border. This distribution of extension would produce the clockwise rotation of the Coast Range and related terrane. Such a distribution would also produce counterclockwise rotation of the Sierra Nevada in addition to simple westward motion. We will return to this point later in the paper. Second, differential extension would require the formation of strike-slip faults separating the regions of greater and lesser extension. The northwest-trending right-lateral faults in Oregon proposed by Lawrence (1976) appear to be such faults (Figure 1). Third, the Columbia River Basalts (Watkins, 1965; Watkins and Baski, 1974) show only 2° of clockwise rotation in northwestern Oregon and southeastern Washington (Figure 2, Table 3) and about 12° of clockwise rotation in south-central Oregon (Figure 2, Table 3). These results would suggest that the southern region has experienced more rotation and extension than the northern region. In fact, the northern region would appear relatively stable and may lie outside the northeastern limit of significant extension and related rotation. However the confidence limits of these paleomagnetic data are too large to permit this interpretation to be made with confidence.

Concerning the timing of the late Tertiary Phase II rotation, the paleomagnetic data are neither abundant nor precise enough to determine exactly when the rotation occurred. However, the regional geology provides additional constraints, since westward motion of the Coast Range, Klamaths and Cascades was undoubtedly associated with extension in regions immediately to the east. It is not until the mid-Miocene that we find clear evidence for broad extension in the region reaching from Arizona to central Oregon. During this period, about 20 m.y.b.p., the Basin and Range province began its most important phase of development with the broad occurrence of extensional faulting coupled with a pervasive shift to basaltic volcanism (Snyder et al., 1976; Stewart, 1978). The most difficult part of the geologic record to interpret is the widespread Oligocene ignimbrites of Nevada and Utah (Snyder et al., 1976), the continuity of which suggests that the Oligocene topography did not include deep extensional basins (Burke and Mckee, 1979). However, Hamilton and Meyers (1966), Elston (1978) and Hamilton (1980) propose that the extrusive ignimbrites were associated with intrusive activity deep in the crust which resulted in significant extension. We conclude, based on the overall geologic record, that Phase II rotation likely began about 20 m.y.b.p., coinciding with mid-Miocene extension in the Basin and Range. However, the possibility of some Oligocene extension in association with the Nevada-Utah ignimbrites cannot be ruled out, so some amount of Oligocene Phase II rotation is possible.

The amount of westward translation of the southern Coast Range, Cascades, and Klamaths required to account for the observed angle of rotation R expressed in radians is related to the distance L from the rotation pivot by:

$$s = L \times R$$

In the preferred Phase II reconstruction (Figure 13), the pivot lies north of the Columbia River, a distance L = 670 km. The angle R can be constrained by the paleomagnetic data. A weighted average of all the rotations observed for Cascade and Coast Range rocks less than 40 m.y. old (post-Phase I) yields $R = 30^{\circ} \pm 10^{\circ}$ (95% confidence). The resulting westward translation of the southern Klamaths, Cascades and Coast Range is s = 340 km. This implies an extension of the Basin and Range on the order of 80%. Although somewhat on the high side, this is within the range of values for the amount of late Cenozoic Basin and Range extension proposed by different researchers (Hamilton and Meyers, 1966; Proffett, 1971; Thompson, 1972; Elston, 1976, 1978; Hamilton, 1978, 1980; Stewart, 1978; Zoback and Thompson, 1978).

The paleogeographic reconstructions we propose are based on two fundamental assumptions which are supported by geologic observations. First, we regard the Coast Range, Klamaths, Cascades and Sierra Nevada as quasi-rigid blocks. As noted in the introduction the regional geology and geophysics suggest a quasi-rigid Coast Range block. Similarly, the consistency in the rotations found for the Cascades (average weighted by 95% confidence limits -- $27^{\circ} \pm 7^{\circ}$, N = 4) and the excellent agreement of these results with the 40

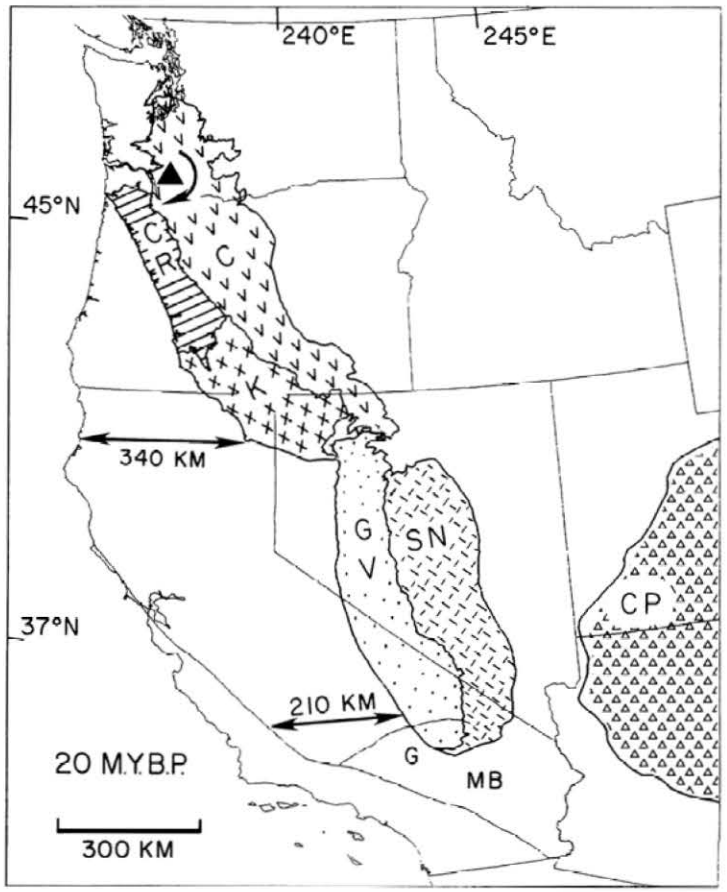

Figure 13. Position of the tectonic blocks of the present western U.S. continental margin at the beginning of Phase II rotation, 20 m.y.b.p. See Figure 1 for the present-day position of these blocks, CP = Colorado Plateau. The rotation pivot at the northern end of the Coast Range block is shown by a triangle. The amounts of Basin and Range extension implied by the model are marked by arrows. The Mojave block (MB) and Garlock Fault (G) are shown in their present-day position.

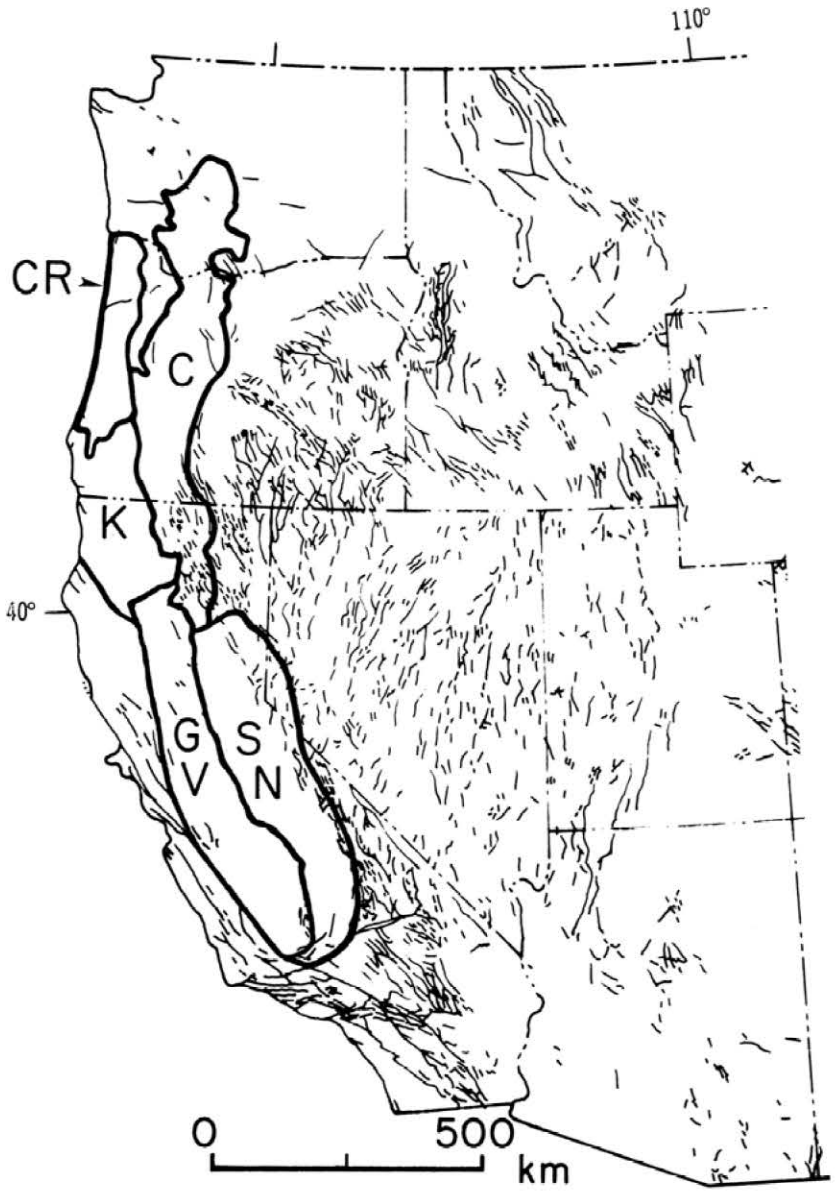

Figure 14. Steeply dipping faults of western North America active in the past 10-15 m.y. for which some Quaternary movement is suspected. Longer faults are generally strike-slip faults and shorter ones normal faults. Our proposed tectonic blocks are outlined with heavy lines; CR = Coast Range, K = Klamaths, GV = Great Valley, SN = Sierra Nevada. Faults are from Eaton (1980). C = Cascades.

m.y. and younger Coast Range rocks (weighted average -- $34^{o} \pm 17^{o}$, N=6) indicate that the Cascades are likely also to be quasi-rigid. In addition, we note that the extensional faults common in the western U.S. occur only sparsely within the Coast Range, Cascades, Klamaths and Sierra Nevada blocks (Figure 14). Regions of high heat flow are confined to the Basin and Range province and the Cascades and are not present in the main mountain belts (Figure 15). These observations suggest a significant contrast in the scales and intensity of late Cenozoic deformation between the Basin and Range and the main mountain belts and provide the basis for our treating the Cascades, Coast Range, Klamaths and Sierra Nevada as coherent blocks in our reconstructions.

The second assumption is that the Sierra Nevada and the Klamaths have not undergone significant translation relative to one another. The widespread occurrence of upper Cretaceous marine sediments in the gap between the Klamaths and Sierra Nevada (Figure 1) is difficult to reconcile with post-Cretaceous rifting of the Klamaths from the Sierra Nevada. Indeed, most geologists working in the area have concluded that rifting of the Klamaths from the Sierra Nevada, if real, occurred during the Mesozoic (Schweikert, 1976; Blake and Jones, 1977; Irwin, 1977). It then appears that the Klamath and Sierra Nevada blocks are likely best described as linked plates (Heptonstall, 1977) free to move about a hypothetical hinge at their point of contact. Such a hinge could accommodate differential westward motion between the Coast Range, Klamaths, Cascades and the Sierra Nevada blocks without significant translation or deformation.

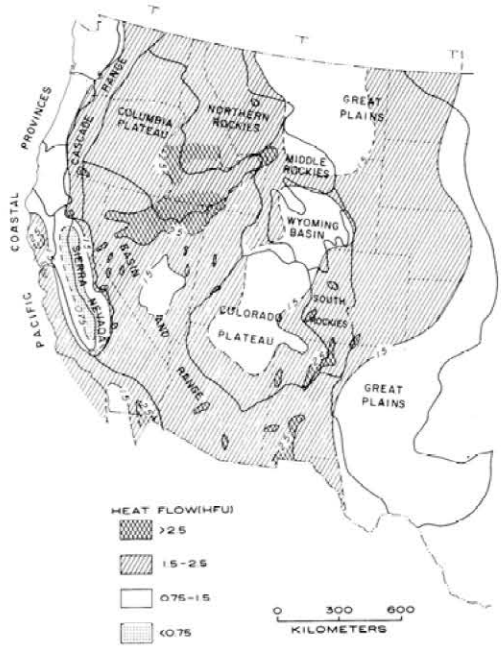

Figure 15. Heat flow contours superimposed on major physiographic units of the western U.S. (Figure from Lachenbruch and Sass, 1978).

PALINSPASTIC MAPS

In order to test whether the above two-phase rotation is consistent with regional geologic information, the palinspastic maps shown in Figures 3 and 13 were generated by the following procedure, working back in time: (1) The outlines of the Coast Range, Klamath Mountains, and Sierra Nevada were digitized along the boundaries between early Tertiary and younger rocks. (2) The Klamath Mountains and the Coast Range of Oregon were rotated counterclockwise about a finite rotation pole at 46.0°N, 237.5°E at a constant rate of 1.5°/m.y. from the present back to 20 m.y., the total rotation angle being 30.4°, in accord with the paleomagnetic data. (The actual rate of rotation was likely spasmodic, associated with periods of pronounced extension and alternate periods of relative stability.) (3) The Sierra Nevada and Great Valley were rotated 13.0° clockwise about a finite rotation pole at 26.9°N, 242.7°E. This preserves the relative position of the northern Sierra Nevada relative to the Klamaths and produces counterclockwise rotation of the Mesozoic paleomagnetic data from the Sierra Nevada. The resultant extension in the southern Basin and Range is 210 km, compared to 340 to the north (Figure 13). (4) All blocks were retained in this position from 20 back to 42 m.y. (5) From 42 back to 50 m.y. the Oregon Coast Range but not the Klamaths was rotated counterclockwise at a rate of 6°/m.y. about a pole to the south located at 43.0°N, 238.7°E, the total rotation angle being 46.0° (Figure 3) in accord with the paleomagnetic data (Figure 12).

Our 20-m.y.b.p. reconstruction agrees well with accepted geodynamic constraints for the western U.S. The rotation pole to the north (Figure 13) preserves general continuity of the Cascade volcanic arc and implies mild compression in the Cascades of southern Washington, likely producing the Miocene uplift of this region (Hammond, 1979). The position of this pole also implies a southwest-northeast opening of the Basin and Range in good agreement with the trend of the Nevada rift (Figure 1) and the orientation of early extensional basins (Eaton, 1979; Zoback and Thompson, 1978). Moreover, the suggested reconstruction of the Sierra Nevada-Great Valley is consistent with accepted geologic constraints. The finite rotation used to determine the early Tertiary position of the Sierra Nevada may, in fact, be decomposed into the three following rotations, each corresponding to a different geologic constraint or observation. The rotations are listed in the sequence in which they were made in order to produce the palinspastic restoration shown in Figure 13. (1) Counterclockwise rotation of 4.0° about a pole at 46.0°N, 237.5°E partially closing the Basin and Range province in partial compensation for Miocene extension. Terrane west of the Basin and Range province, including the Sierra Nevada and Mojave blocks, were moved eastward in this restoration. This same pole position with a larger rotation was used to produce the 20-m.y.b.p. restoration of the Oregon Coast Range. (2) As-

suming that motion along the Walker Lane reflects strike-slip motion between the North American (NA) and Pacific (PAC) plates, this motion can be described by the PAC-NA pole at 51.0°N, 294.0°E of Minster et al. (1974). Clockwise rotation of 1.2° about this pole produces right-lateral motion of 90 km along the Walker Lane, in good agreement with geologic observations (Albers, 1967; Slemmons et al., 1979). A counterclockwise rotation of 1.2° was therefore used in the reconstruction. (3) Left-lateral motion along the Garlock Fault can be described by a pole at 33.0°N, 243.5°E. Counterclockwise rotation of 17.0° about this pole produces 85 km of left-lateral motion on the Garlock and related faults to the south, which is consistent with geologic observations (Davis and Burchfiel, 1973). A clockwise rotation of 17.0° about this pole was used to move the Sierra Nevada east relative to the Mojave block to its position prior to differential Basin and Range extension. These three rotations carried out in the sequence listed above are exactly equivalent to the rotation about the single pole used to produce the reconstruction of the Sierra Nevada block (Figure 13). Because the rotation in step (2) is small, the sequence in which steps (1) and (2) are made is not important. These two combined rotations were used to rotate the Sierra Nevada block, the Mojave block and the pole for the intervening Garlock Fault. Holding the Mojave block fixed, the Sierra Nevada block was then rotated relative to the Mojave block about the rotated Garlock Fault pole. A remarkably similar three-pole system was derived independently by Eaton (1979) on the basis of the distribution and direction of extension in the Basin and Range. The fact that several of the primary geotectonic features of the Basin and Range and western U.S. can be explained by a reconstruction based mainly on paleomagnetic constraints lends considerable credibility to the reconstruction.

ALTERNATIVE MODELS

How well the positions of the major mountain blocks can be determined at 20 m.y.b.p. depends upon uncertainties in the amount of Basin and Range extension and in the orientation of the Sierra Nevada block. The orientation of the Sierra Nevada block can be constrained loosely by the paleomagnetic data from the block. As can be seen in Figure 13, our 20-m.y.b.p. reconstruction proposes a 13° rotation of the Sierra Nevada about a pole at 26.9°N, 242.7°E, which should be reflected in the paleomagnetic data as a 15° counterclockwise rotation of pre- late Tertiary field directions. Paleomagnetic studies of Mesozoic rocks of the Sierra Nevada and Great Valley (Figure 1, Table 3) are consistent with a small counterclockwise rotation of $4.4^{\circ} \pm 5.7^{\circ}$ (95% confidence limits). However two facts should be kept in mind regarding the accuracy of this mean result. First, two of the magnetic studies were on rocks which have undergone post-folding remagnetization events and hence have unconstrained tectonic tilt corrections. Second, all the individual rotational uncertainties are between 14° and 23° (Table 3) and hence introduce considerable uncertainty to the derived mean rotation.

The reason our favored 20-m.y.b.p. reconstruction does not utilize a Sierra Nevada rotation closer to 4.4° rather than 15° is that smaller Sierra Nevada rotations result in unacceptable positions for the southern Sierra Nevada. The present gap between the southern Sierra Nevada and the Colorado Plateau is approximately 360 km wide and in that gap there is about 215 km of post-Cretaceous surface outcrop. This sets a likely Tertiary extension upper limit of 215 km (150%) in this region. Our preferred reconstruction assumes that extension was equal to this upper limit. For a given rotation of the Coast Range, Cascades, and Klamaths, there is a simple trade-off between implied extension in the southern Basin and Range and rotation of the Sierra Nevada. Clearly one may propose a smaller amount of extension in the region of the southern Sierra Nevada, but the implied Sierra Nevada rotation increases by 1.5° for every 20 km of extension less than 215 km. Figure 16 shows an alternative 20-m.y.b.p. reconstruction based on a 30° clockwise rotation of the Coast Range-Klamaths-Cascades and a 4.4° counterclockwise rotation of the Sierra Nevada. Note the unacceptable proximity of the southern Sierra Nevada to the Colorado Plateau, implying 340 km of Tertiary extension, 125 km greater than the upper limit.

Alternative models which yield acceptable Sierra Nevada rotation and positions of the southern Sierra Nevada involve moving the Cascade-Klamath pivot to the south or reducing the amount of proposed Phase II rotation. Both alternatives lessen translation of the northern Sierra Nevada and produce less Sierra Nevada-Great Valley rotation for a given position of the southern Sierra Nevada. We do not favor these alternative models, since

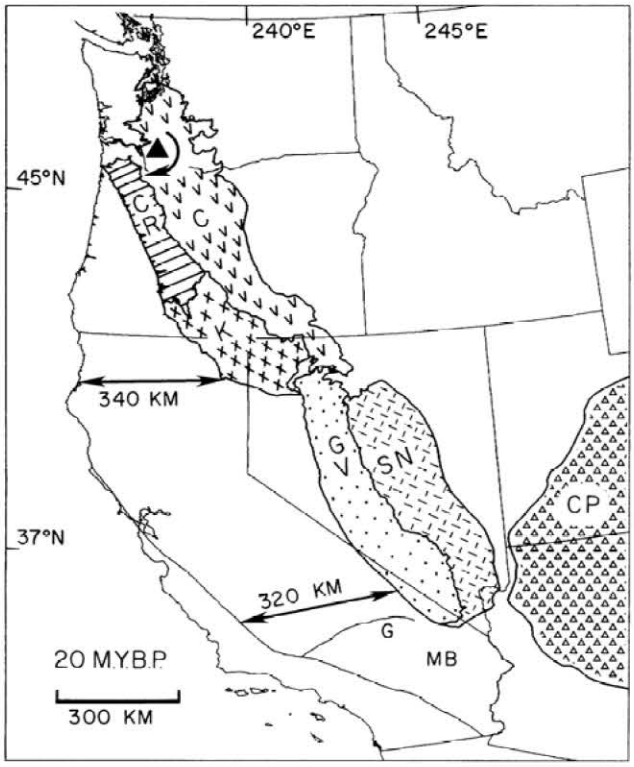

Figure 16. Alternative Phase II reconstruction decreasing the counterclockwise rotation of the Sierra Nevada to 4.4° but yielding an unacceptable proximity of the southern Sierra Nevada (SN) to the Colorado Plateau (CP).

each has unacceptable geologic implications. Moving the Coast Range-Cascade-Klamath pivot to the south as little as 160 km (Figure 17) would reduce implied extension in the northern Basin and Range to 260 km (50%) and result in only 6° counterclockwise rotation for the same position of the southern Sierra Nevada as our preferred model (Figure 13). However the implication of the more southerly pivot is nearly 180 km of compression east of the north Cascades as the Cascades rotate. The relatively undeformed character of the Columbia River Basalts (largely pre-Basin and Range extension) in central Washington and only moderate folding in the Cascades themselves (Hammond, 1979) appears to preclude such massive compression.

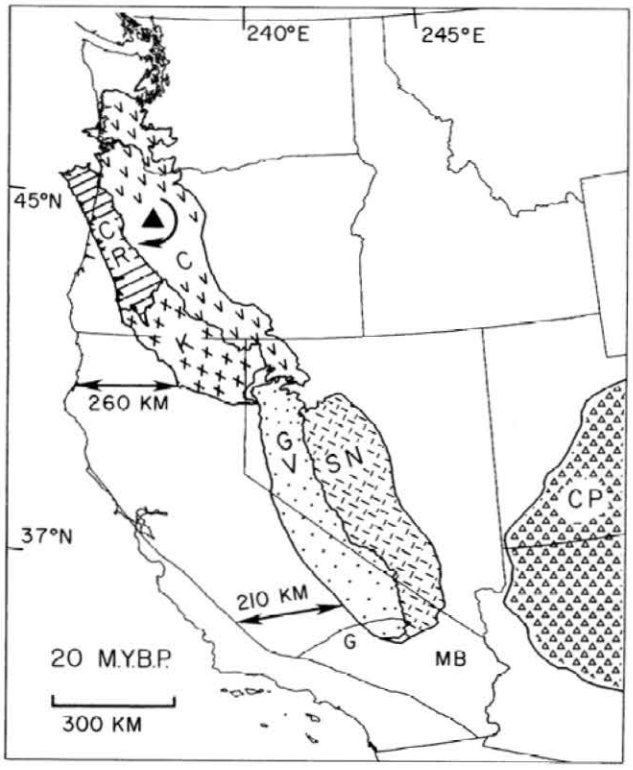

Figure 17. Alternative Phase II reconstruction moving the pivot south to 44.5° N 237.5° E. Less rotation of the Sierra Nevada (4.4° counterclockwise) and less extension of the Basin and Range (50%) is required in this model, but the implied compression in the Cascades of southern Washington is unacceptably large.

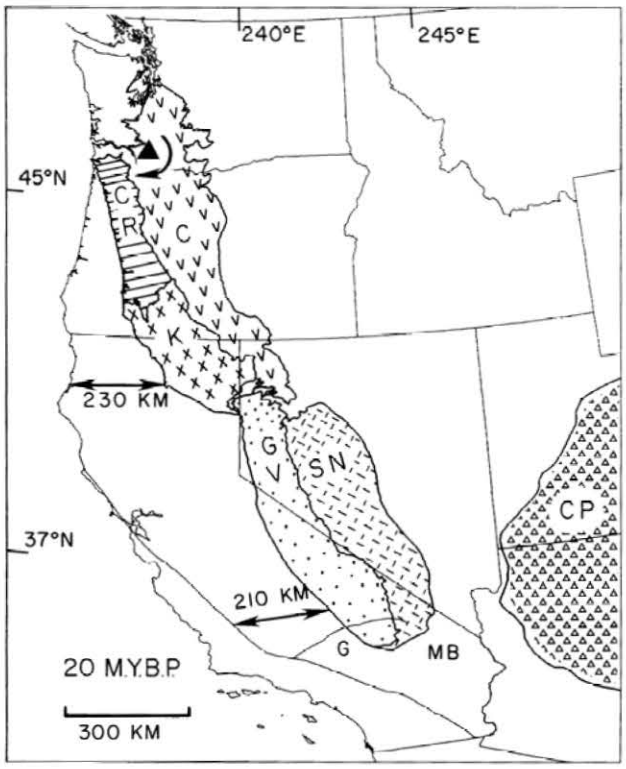

Figure 18. Alternative Phase II reconstruction reducing the proposed rotation of the Coast Range, Cascades, Klamaths to 20°; less Basin and Range extension (40%) and less Sierra Nevada rotation (4.4° counterclockwise) results.

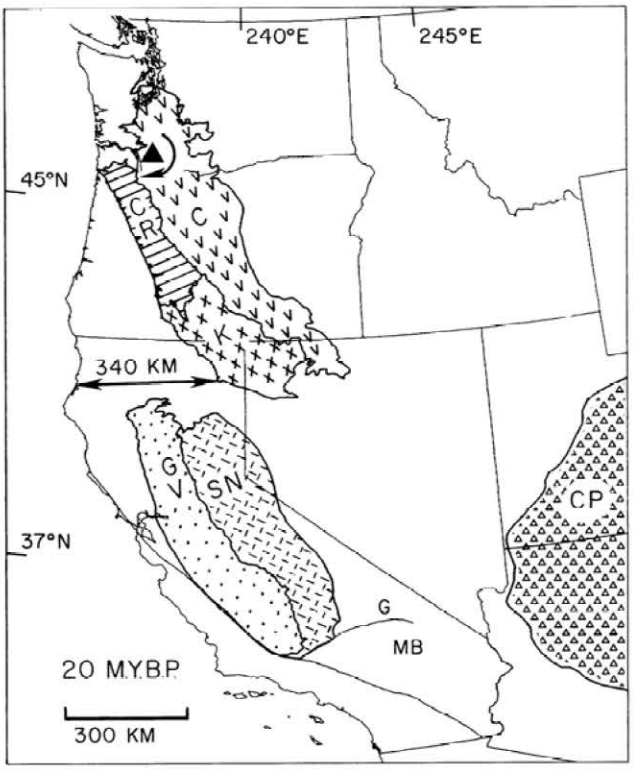

Figure 19. Alternative Phase II reconstruction relaxing our assumption of no Klamath - Sierra Nevada relative translation, rotating the Coast Range, Cascades and Klamaths 30.4° and holding the Sierra Nevada - Great Valley fixed. Note the large distance separating the northern Great Valley from the Klamaths.

Reducing the proposed rotation of the Coast Range-Cascade-Klamath block ($30^{\circ} \pm 10^{\circ}$) to its lower statistical bound of 20° results in only 4.4° of counterclockwise rotation of the Sierra Nevada (Figure 18) for the same southern Sierra Nevada position as in our preferred model (145 km west of the Colorado Plateau). Although apparently satisfactory, this model implies a Coast Range rotation smaller than the 95% confidence limits on the Coast Range Oligocene intrusives ($44.5^{\circ} \pm 16.7^{\circ}$) and the Yachats Basalt ($54.7^{\circ} \pm 30.2^{\circ}$) allow. We suggest that realistic error limits on the Phase II rotation are $\pm 3^{\circ}$ rather than $\pm 10^{\circ}$. It is our judgement that the Coast Range paleomagnetic directions are of higher quality than the Sierra Nevada data, and therefore any model should be consistent with the Coast Range data even if consistency with the Sierra Nevada data must be lessened. It should be noted however that our preferred Phase II reconstruction Sierra Nevada rotation of 15° is still within all the 95% confidence limits of the individual Sierra Nevada-Great Valley rotations, even though in excess of the 95% confidence limits of the data taken as a group.

Our final option to lessen rotation of the Sierra Nevada implied by our reconstructions is to reject our assumption of no Klamath-Sierra Nevada translation. Figure 19 shows a reconstruction leaving the Sierra Nevada in its present position and rotating the Coast Range-Cascades-Klamaths as in our preferred model. Figure 20 shows the consequences of this reconstruction at 10 m.y.b.p., assuming a uniform rotation rate. The Klamaths and Sierra Nevada collide in such a model and would greatly deform the southern Klamaths and the Cretaceous sediments which presently occupy the gap between the Sierra Nevada and the Klamaths. Such deformation has not been found in the region, and hence this model is rejected. Consequences are similar even if the Sierra Nevada is moved east in partial compensation for Basin and Range extension. Such compensation merely results in an earlier (pre-10 m.y.b.p.) collision of the Klamaths and Sierra Nevada.

It is our conclusion that there are alternative reconstructions to our preferred model, but there are serious geologic consequences implied by radical changes. Clearly some changes are possible, including (1) a small amount of Klamath-Sierra Nevada relative translation, (2) a southern Sierra Nevada translation somewhat less than 215 km, (3) moving the northern pivot a small distance to the south, (4) rotating the Coast Range, Klamaths, and Cascades slightly less than 30° (Phase II), and (5) rotating the Sierra Nevada a few degrees more or less than 15°. However, it is our judgement that any of the above adjustments must be small and hence of second order significance, since large adjustments are hard to reconcile with the geology.

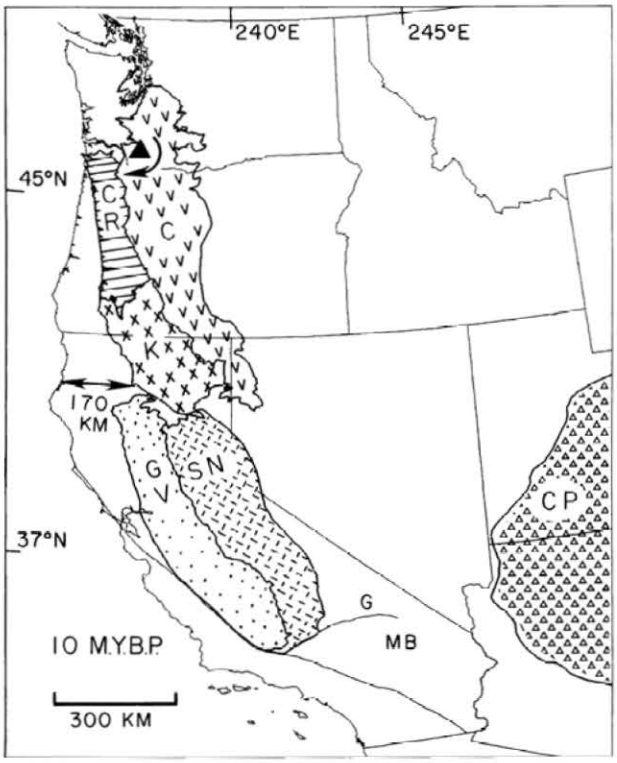

Figure 20. Alternative Phase II reconstruction of Figure 19 stepped forward in time to 10 m.y.b.p. Note the resulting collision of the southern Klamaths with the northern Sierra Nevada.

DISCUSSION AND SPECULATIONS

During Phase II rotation the direction of motion of the Klamath-Sierra Nevada junction appears to be the resultant of two components, one southwesterly and one northwesterly. The southwesterly component is due to the extension of the Basin and Range province, which appears to be a continental analogue of broadly distributed back-arc spreading. This appears to be necessary to explain the high heat flow, thin crust, anomalous upper mantle and regional uplift of the Basin and Range (Scholz et al., 1971; Thompson, 1972). The northwesterly compoment of motion is associated with broad regional right-lateral shear (Atwater, 1970; Christiansen and Mckee, 1978; Livaccari, 1979; Zoback and Thompson, 1978). The late Cenozoic right-lateral motion (48 km minimum) along the Walker Lane (Albers, 1967; Slemmons et al., 1979) requires north-northwest motion of the Sierra Nevada relative to the stable part of the North American plate. Regional shear reflected in the northwesterly motion of the Sierra Nevada and adjacent terrane to the east would appear to be the likely cause of Miocene to present north-south compression in the Columbia Plateau (see Davis, 1977) as the plateau is pushed from the south against a more stationary Mesozoic terrane to the north. A similar buttress effect likely constrains the Coast Range and Cascades to the north, as evidenced by north-south compressional earthquakes (see Davis, 1977) in Washington and northern Oregon. The Phase II rotation of the Coast Range, Klamaths and Cascades would thus appear to be the result of southwesterly Basin and Range extension with superimposed northwesterly motion of the Sierra Nevada, both acting to push the Coast Range, Klamaths and Cascades in a northwesterly clockwise sense about a northern pivot.

The implication of rotation of the continental margin is that a buttress does not exist to the west, since the Coast Range, Klamaths and Cascades must translate to the west during rotation. This translation appears to have been accommodated by the Juan de Fuca-North America trench, with the continental margin simply overriding the trench during rotation. It is of significance that during extension of the Basin and Range and Phase II rotation the continental margin west of the Sierra Nevada and Coast Range has been associated with a trench (Atwater, 1970), a trench being the only type of continental boundary capable of absorbing a translating continental margin.

The Juan de Fuca ridge has rotated 23° relative to the Pacific plate during the past 10 m.y. in the same clockwise sense as the Coast Range (Figure 21), raising the intriguing possibility that the rotation of the western continental margin may have been the cause of ridge rotation. If there had been strong coupling between the adjacent continental and oceanic plates, then one might expect concurrent rotation of the Juan de Fuca plate with the adjacent continental block during the past 20 m.y. The marine magnetic anomalies

clearly indicate that the plate interactions have been more complicated than simple rotation. In particular, anomalies 4 and 5 (7 and 10 m.y.) on the Pacific plate trend N 4° W whereas the corresponding anomalies on the Juan de Fuca plate trend N 6° E, establishing that this plate has rotated clockwise no more than 10° relative to the Pacific plate (Figure 21). In view of the negligible rotation between the Pacific and North American plates during the past 10 m.y., the anomalies preclude rotation of the Juan de Fuca plate by an angle much greater than 10° during the past 10 m.y. This rotation may have been produced by coupling of the Juan de Fuca and Gorda plates to the rotating continental margin. However, the Juan de Fuca-Gorda ridge has undergone a much larger rotation of approximately 23° relative to anomalies 4 and 5 on the Pacific plate. If the 23° ridge rotation were due entirely to rotation of the Juan de Fuca and Gorda plates about a local Euler pole, the Juan de Fuca and Gorda anomalies (4, 5) should be rotated 46° relative to the Pacific

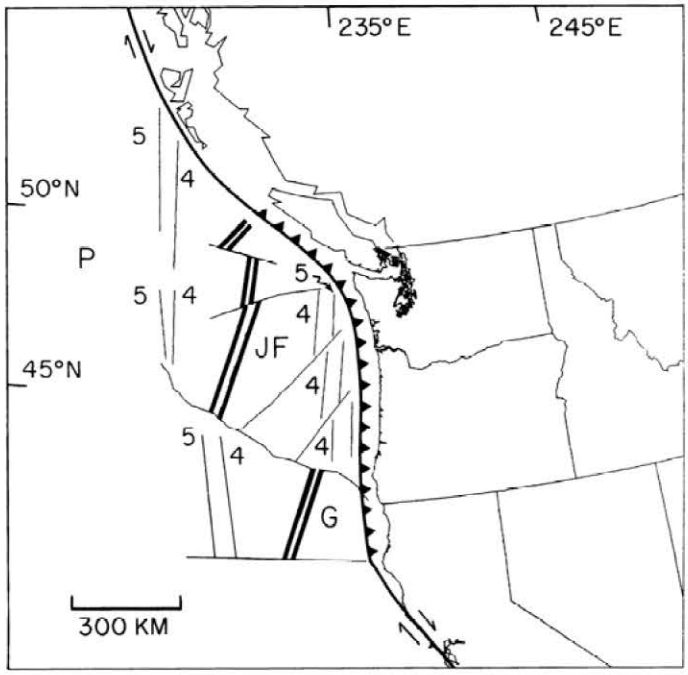

Figure 21. Ridge geometry and magnetic anomalies associated with the Pacific, Juan de Fuca and Gorda plates. Anomalies 4 (7 m.y.) and 5 (10 m.y.) are shown for both the Pacific and Juan de Fuca plates. P = Pacific plate, JF = Juan de Fuca plate, G = Gorda plate. Map is based on Atwater and Menard (1970) and Hays and Pitman (1970).

anomalies, whereas only 10^{o} is observed. The increasing divergence between the ridge and the nearly parallel older anomalies on either side indicate that some process is occurring other than simple rotation of two rigid plates. It is interesting to note that if the mid-Tertiary trench was parallel to the northwest trend of our Phase II continental margin, then the angle between the ridge and the trench has remained more nearly constant than it would have if the ridge had not changed orientation. Gordon et al. (1978) have pointed out that the direction of plate motion is mainly controlled by the location of a plate's trench system. Their analysis would predict that a clockwise rotation of the trench between the Juan de Fuca plate and North America would have the result of changing the direction of motion of the Juan de Fuca plate in a clockwise direction, for example, from a northeasterly to an easterly direction. It is interesting to speculate that the change in azimuth of the Juan de Fuca ridge reflects changes in the direction of motion of the Juan de Fuca plate. The latter, in turn, may reflect changes in the orientation and length of the trench as the Pacific-North America-Juan de Fuca triple junction migrated northward (Atwater, 1970) along a trench that was migrating westward and rotating in a clockwise direction.

ACKNOWLEDGEMENTS

We would like to thank A. McBirney and J. Smith for assistance in selecting sampling locations within the Western Cascades and for helpful discussions about the regional structure, geology and geochronology. We also would like to thank G.Thrupp for assistance in collecting rock samples and W. Dickinson, Z. Ben-Avraham, P.D. Snavely and D. Engebretson for helpful discussions. This research was funded by Grant EAR 79-19712 from the National Science Foundation, Grant PRF 11405-AC2 from the Petroleum Research Fund, and under U.S. Department of Energy contract DE FC 07-79-ID-12044.

REFERENCES

Albers, J.P., 1967, Belt of sigmoidal bending and right-lateral faulting in the western Great Basin: Geol. Soc. Am. Bull., v. 78, p. 143-156.

Atwater, T., 1970, Implications of plate tectonics for the Cenozoic tectonic evolution of western North America: Geol. Soc. America Bull., v. 81, p. 3513-3536.

Atwater, T., and Menard, H.W., 1970, Magnetic lineations in the north-east Pacific: Earth Planetary Sci. Letters, v. 7, p. 445-450.

Baldwin, E.M., 1964, Thrust faulting in the Roseburg area, Oregon: Ore Bin, v. 26, p. 176-184.

Baldwin, E.M., 1974, Eocene stratigraphy of southwestern Oregon: Oregon Dept. Geol. and Min. Ind. Bull. 83, 40 p.

Baldwin, E.M., 1975, Revision of the Eocene stratigraphy of southwestern Oregon: Paleogene symposium, Pac. Sec., Am. Soc. Petroleum Geol. - Soc. Econ. Paleontologists and Mineralogists - Soc. Explor. Geophys. Annual Meeting, p. 49-64.

Bates, R.G., and Beck, M.E., Jr., in press, Tectonic rotations in the Cascade Mountains of southern Washington: Geology.

Bates, R.G., Beck, M.E., Jr., and Simpson, R.W., 1979, Preliminary paleomagnetic results from the southern Cascade range of southwestern Washington [abs.]: EOS (Am. Geophys. Union Trans.), v. 60, p. 816-817.

Beaulieu, J.D., 1971, Geologic formations of western Oregon west of longitude 120° 30': Oregon Dept. Geol. and Min. Ind. Bull. 70, 72p.

Beck, M.E., Jr., 1962, Paleomagnetism of a thick Tertiary volcanic sequence in northern California: U.S.A.F. Cambridge Research Laboratory Report AFCRL 62-821, 45p.

Beck, M.E., Jr., and Burr, C.D., 1979, Paleomagnetism and tectonic significance of the Goble Volcanic Series, southwestern Washington: Geology, v. 7, p. 175-179.

Beck, M.E., Jr., Engebretson, D.C., Gromme, C.S., Taylor, E.M., and Whitney, J.W., 1978, Paleomagnetism of the middle Tertiary Clarno Formation, north-central Oregon: constraint of the models for tectonic rotation [abs.]: EOS, (Am. Geophys. Union Trans.), v. 59, p. 1058.

Beck, M.E., Jr., and Plumley, P., in press, Paleomagnetism of intrusive rocks in the Coast Range of Oregon: microplate rotations in the middle Tertiary: Geology.

Berg, J.W., Jr., Trembly, L., Emilia, S.A., Hutt, J.R., King, J.M., Long, L.T., McKnight, W.R., Sarmah, S.K., Souders, R., Thiruvathukal, J.V., and Vossler, D.A., 1966, Crustal refraction profile, Oregon Coast Range: Seismol. Soc. America Bull., v. 56, p. 1357-1362.

Blake, M.C., Jr., and Jones, D.L., 1977, Tectonics of the Yolla Bolly Junction and its significance to the plate tectonic history of northern California [abs.]: Geol. Soc. America Abs. with Programs, v. 9, p. 391.

Bromery, R.W., and Snavely, P.D., Jr., 1964, Geologic interpretation of reconnaissance gravity and aeromagnetic surveys in northwestern Oregon: U.S. Geol. Survey Bull. 1181-N, p. N1-N13.

Burke, D.B., and McKee, E.H., 1979, Mid-Cenozoic volcano-tectonic troughs in central Nevada: Geol. Soc. America Bull., Part I, v. 90, p. 181-184.

Cady, W.M., 1975, Tectonic setting of the Tertiary volcanic rocks of the Olympic Peninsula, Washington: U.S. Geol. Survey Jour. Res., v. 3, p. 573-582.

Clark, H.C., 1969, Remanent magnetization, cooling history, and paleomagnetic record of the Marys Peak sill, Oregon: Jour. Geophys. Res., v. 74, p. 3143-3160.

Cohee, G.V. (compiler), 1962, Tectonic map of the United States, exclusive of Alaska and Hawaii: U.S. Geol. Survey and Am. Assoc. Petroleum Geologists.

Christiansen, R.L., and McKee, E.H., 1978, Late Cenozoic volcanic and tectonic evolution of the Great Basin and Columbia intermontane region, *In* Smith, R.B., and Eaton, G.P., eds., Cenozoic Tectonics and Regional Geophysics of the Western Cordillera: Geol. Soc. America Mem. 152, p. 283-311.

Davis, G.A., 1977, Tectonic evolution of the Pacific Northwest: Precambrian to present: Washington Public Power Supply System, Nuclear Proj. No. 1, Subappendix 2RC, PSAR, Ammendment 23, p.i-2R C-46.

Davis, G.A., and Burchfiel, B.C., 1973, Garlock fault: an intercontinental transform structure, southern California: Geol. Soc. America Bull., v. 84, p. 1407-1422.

Davis, G.A., Monger, J.W.H., and Burchfiel, B.C., 1978, Mesozoic construction of the Cordilleran "collage" central British Columbia to central California, *In* Howell, D.G., and McDougall, K.A. eds., Mesozoic Paleogeography of the Western United States: Pacific Section, SEPM, p. 1-32.

Dickinson, W.R., 1976, Sedimentary basins developed during evolution of Mesozoic-Cenozoic arc-trench system in Western North America: Can. Jour. Earth Sci., v. 13, p. 1268-1287.

Eaton, G.P., 1979, A plate-tectonic model for late Cenozoic crustal spreading in the western United States, *In* Riecker, R.E., ed., Rio Grande Rift - Tectonics and Magnetism: Am. Geophys. Union, p. 7-32.

Eaton, G.P., 1980, Geophysical and geological characteristics of the crust of the Basin and Range province, *In* Continental Tectonics, Studies in Geophysics: National Academy of Sciences, p. 96-113.

Elston, W.E., 1976, Tectonic significance of mid-Tertiary volcanism in the Basin and Range Province: a critical review with special reference to New Mexico, *In* Cenozoic Volcanism in Southwestern New Mexico: New Mexico Geol. Soc. Spec. Pub. 5, p. 93-151.

Elston, W.E., 1978, Rifting and volcanism in the New Mexico segment of the Basin and Range, southwestern U.S.A., *In* Neuman, E.R., and Ramberg, I.B., eds., Petrology and Geochemistry of Continental Rifts: Dordrecht, Holland, D. Reidel, p. 79-86.

Garrison, R.E., 1973, Space-time relations of pelagic limestones and volcanic rocks, Olympic Peninsula, Washington: Geol. Soc. America Bull., v. 84, p. 583-594.

Glassley, W.E., 1974, Geochemistry and tectonics of the Crescent volcanic rocks, Olympic Peninsula, Washington: Geol. Soc. America Bull., v. 85, p. 785-794.

Globerman, B.R., and Beck, M.E., Jr., 1979, Cenozoic tectonic rotations in the western

cordillera: new evidence from the Washington Coast Range [abs.]: EOS (Am. Geophys. Union Trans.), v. 60, p. 817.

Gordon, R.G., Cox, A., and Harter, C.E., 1978, Absolute motion of an individual plate estimated from its ridge and trench boundaries: Nature, v. 274, p. 752- 755.

Gromme, C.S., and Merrill, R.T., 1965, Paleomagnetism of Late Cretaceous granitic plutons in the Sierra Nevada, California: further results: Jour. Geophys. Res., v. 70, p. 3407-3420.

Gromme, C.S., Merrill, R.T., and Verhoogen, J., 1967, Paleomagnetism of Jurassic and Cretaceous plutonic rocks in the Sierra Nevada, California, and its significance for polar wandering and continental drift: Jour. Geophys. Res., v. 72, p. 5661-5684.

Hamilton, W., 1969, Mesozoic California and the underflow of Pacific Mantle: Geol. Soc. America Bull., v. 80, p. 2409-2430.

Hamilton, W., 1978, Mesozoic tectonics of the Western United States, *In* Howell, D.G., and McDougall, K.A., eds., Mesozoic Paleogeography of the Western United States: Pacific section, SEPM, p. 33-70.

Hamilton, W., 1980, Complexities of modern and ancient subduction systems, *In* Continental Tectonics, Studies in Geophysics: National Academy of Sciences, p. 33-41.

Hamilton, W., and Meyers, W.B., 1966, Cenozoic tectonics of the Western United States: Rev. Geophys., v. 4, p. 509-540.

Hammond, P.E., 1979, A tectonic model for evolution of the Cascade Range, *In* Armentrout, J.M., Cole, M.R., and Terbest, H., Jr., eds., Cenozoic Paleogeography of the Western United States: SEPM, p. 219-237.

Hannah, J.L., and Verosub, K.L., 1979, Paleomagnetism of late Paleozoic strata of the northern Sierra Nevada, California, and its implications for Mesozoic and Cenozoic tectonics: Geol. Soc. America Abs. with Programs, v. 11, p. 537.

Hays, D.E., and Pitman, W.C. III, 1970, Magnetic lineations in the N. Pacific, *In* Hays, J.D., ed., Geological Investigations of the N. Pacific: Geol. Soc. America Memoir 126, p. 291-314.

Heptonstall, W.B., 1977, Plate linkage mechanism to account for oroclinal deformation in the western cordillera of North America: Nature, v. 268, p. 27-32.

Hoover, L., 1963, Geology of the Anlauf and Drain quadrangles, Douglas and Lane counties, Oregon: U.S. Geol. Survey Bull. 1122-D, 62p.

Huntting, M.T., Bennett, W.A.G., Livingston, V.E., Jr., and Moen, W.S., 1961, Geologic map of Washington: Washington Department of Conservation, Division of Mines and Geology.

Irving, E., 1979, Paleopoles and paleolatitudes of North America and speculations about displaced terrains: Can. Jour. Earth Sci., v. 16, p. 660-694.

Irwin, W.P., 1977, Review of Paleozoic rocks of the Klamath Mountains, *In* Paleozoic Paleogeography of the Western United States, Pacific Coast Paleogeography Symp. I: Soc. Econ. Paleontologists and Mineralogists, p. 441-454.

Lachenbruch, A.H., and Sass, J.H., 1978, Models of an extending lithosphere and heat flow in the Basin and Range province, *In* Smith, R.B. and Eaton, G.P., eds., Cenozoic Tectonics and Regional Geophysics of the Western Cordillera: Geol. Soc. America Memoir 152, p. 209-250.

Langston, A., and Blum, D.E., 1977, The April 29, 1965, Puget Sound earthquake and the crustal and upper mantle structure of western Washington: Seismol. Soc. America Bull., v. 67, p. 693-712.

Lawrence, R.D., 1976, Strike-slip faulting terminates the Basin and Range Province in Oregon: Geol. Soc. America Bull., v. 87, p. 846-850.

Livaccari, R.F., 1979, Late Cenozoic tectonic evolution of the western United States: Geology, v. 7, p. 72-75.

Loeschke, J., 1979, Basalts of Oregon (U.S.A.) and their geotectonic environment, I. Petrochemistry of Tertiary basalts of the Oregon Coast Range: Neues Jahrbuch für Mineralogie, Abhandlungen, v. 134, p. 225-247.

Lovell, J.P.V., 1969, Tyee Formation: undeformed turbidites and their lateral equivalents, mineralogy and paleogeography: Geol. Soc. America Bull., v. 80, p. 9-22.

Magill, J.R., Cox, A.V., and Duncan, R., in press, Tillamook Volcanic Series: further evidence for tectonic rotation of the Oregon Coast Range: Jour. Geophys. Res.

Mankinen, E.A., 1978, Paleomagnetic evidence for a late Cretaceous deformation of the Great Valley sequence, Sacramento Valley, California: U.S. Geol. Survey Jour. Res., v. 6, p. 383-390.

Minster, J.B., Jordan, T.H., Molnar, P., and Haines, E., 1974, Numerical modeling of instantaneous plate tectonics: Royal Astron. Soc. Geophys. Jour., v. 36, p. 541-576.

Nelson, D.O., and Shearer, G.B., 1969, The geology of Cedar Butte, northern Coast Range of Oregon: Ore Bin, v. 31, p. 113-130.

Peck, D.L., Griggs, A.B., Schlicker, H.G., Wells, F.G., and Dole, H.M., 1964, Geology of the central and northern parts of the Western Cascade Range in Oregon: U.S. Geol. Survey Prof. Paper 449, 56p.

Proffett, T.M., Jr., 1971, Late Cenozoic structure in the Yerington district, Nevada, and the origin of the Great Basin: Geol. Soc. America Abs. with Programs, v. 3, p. 181.

Roberts, A.E., 1958, Geology and coal resources of the Toledo-Castle Rock district, Cowlitz and Lewis counties, Washington: U.S. Geol. Survey Bull. 1062, 71p.

Schweikert, R.A., 1976, Early Mesozoic rifting and fragmentation of the Cordilleran orogen in the western U.S.A.: Nature, v. 260, p. 586-591.

Scholz, C.H., Barazangi, M., and Sbar, M.L., 1971, Late Cenozoic evolution of the Great Basin, western United States, as an ensialic interarc basin: Geol. Soc. America Bull., v. 82, p. 2979-2990.

Seno, T., 1977, The instantaneous rotation vector of the Philippine Sea plate relative to the Eurasian plate: Tectonophysics, v. 42, p. 209-226.

Simpson, R.W., 1977, Paleomagnetic evidence for tectonic rotation of the Oregon Coast Range: Stanford University, Ph.D. dissert., 156p.

Simpson, R.W., and Cox, A., 1977, Paleomagnetic evidence for tectonic rotation of the Oregon Coast Range: Geology, v. 5, p. 585-589.

Slemmons, D.B., Van Wormer, D., and Bell, E.J., 1979, Recent crustal movements in the Sierra Nevada - Walker Lane region of California-Nevada, Part I, Rate and style of deformation: Tectonophysics, v. 52, p. 561-570.

Snavely, P.D., Jr., Brown, R.D., Jr., Roberts, A.E., and Rau, W.W., 1958, Geology and coal resources of the Centralia-Chehalis District, Washington: U.S. Geol. Survey Bull. 1053, 159p.

Snavely, P.D., Jr., and MacLeod, N.S., 1974, Yachats Basalt - an upper Eocene differentiated volcanic sequence in the Oregon Coast Range: U.S. Geol. Survey Jour. Res., v. 2, p. 395-403.

Snavely, P.D., Jr., MacLeod, N.S., and Rau, W.W., 1970, Summary of the Tillamook area, Northern Oregon Coast Range: U.S. Geol. Survey Prof. Paper 650-A, p. A47.

Snavely, P.D., Jr., MacLeod, N.S., and Wagner, H.C., 1968, Tholeiitic and alkalic basalts of the Eocene Siletz River volcanics, Oregon Coast Range: Am. Jour. Sci., v. 266, p. 454-481.

Snavely, P.D., Jr., and Wagner, H.C., 1963, Tertiary geologic history of western Oregon and Washington: Wash. Div. Mines and Geol. Report Inv. 22, 25p.

Snavely, P.D., Jr., Wagner, H.C., and MacLeod, N.S., 1964, Rhythmic-bedded eugeosynclinal deposits of the Tyee Formation, Oregon Coast Range: Kansas Geol. Survey Bull. 169, v. 11, p. 461-480.

Snyder, W.S., Dickinson, W.R., and Silberman, M.L., 1976, Tectonic implications of the space-time patterns of Cenozoic magmatism in the western United States: Earth Planetary Sci. Letters, v. 32, p. 91-106.

Stewart, J.H., 1978, Basin and range structures in western North America, a review, *In* Smith, R.B., and Eaton, G.P., eds., Cenozoic Tectonics and Regional Geophysics of the Western Cordillera: Geol. Soc. America Memoir 152, p. 1-31.

Tatel, H.E., and Tuve, M.A., 1955, Seismic exploration of a continental crust: Geol. Soc. America Spec. Paper 62, p. 35-50.

Thompson, G.A., 1972, Cenozoic Basin and Range tectonism in relation to deep structure: Internat. Geol. Cong. Proc. 24th Montreal, p. 84-90.

Walker, G.W., 1977, Geologic map of Oregon east of the 121st meridian: U.S. Geol. Survey Map I-902.

Watkins, N.D., 1965, Paleomagnetism of the Columbia Plateaus: Jour. Geophys. Res., v. 70, p. 1379-1406.

Watkins, N.D., and Baski, A.K., 1974, Magnetostratigraphy and oroclinal folding of the Columbia River, Steens and Owyhee basalts in Oregon, Washington and Idaho: Am. Jour. Sci., v. 274, p. 148-189.

Wells, F.G., and Peck, D.L., 1961, Geologic map of Oregon west of the 121st meridian: U.S. Geol. Survey Map I-325.

Wells, R.E., and Coe, R.S., 1979, Paleomagnetism and tectonic significance of the Eocene Crescent Formation, southwestern Washington [abs]: Geol. Soc. America Abs. with Programs, v. 11, p. 537-538.

White, C.M., and McBirney, A.R., 1979, Tholeiitic lavas from the basal portion of the Western Cascade sequence in Oregon [abs.]: Pacific Northwest Meeting of the Am. Geophys. Union, Bend, Oregon.

Wilkinson, W.D., Allen, J.E., Lowell, W., Lowry, W., Hutchinson, M., Harper, H., Littleton, R., Meade, R., and Jones, S., 1941, Reconnaissance geologic map of the Butte Falls quadrangle, Oregon: Oregon Dept. Geol. and Min. Ind. Bull. 22.

Williams, H., 1949, Geology of the Macdoel quadrangle: California Division of Mines Bulletin 151, 71p.

Wise, W.S., 1969, Geology and petrology of the Mt. Hood area: a study of High Cascade volcanism: Geol. Soc. America Bull., v. 80, p. 969-1006.

Zoback, M.L., and Thompson, G.A., 1978, Basin and Range rifting in northern Nevada: clues from a mid-Miocene rift and its subsequent offsets: Geology, v. 6, p. 111-116.

APPENDICES

Appendix 1. Compilation of paleomagnetic data from the Western Cascades

Sample	*Declination*	*Inclination*	*Intensity (emu/cc)*	*Demagnetization (mT)*
S001-0*	342.6	64.9	2.18 x 10-3	0
	345.6	63.9	1.90 x 10-3	5
	356.2	65.9	1.59 x 10-3	10
	16.1	69.3	1.16 x 10-3	20
	16.6	69.3	1.15 x 10-3	20
	28.3	69.1	8.63 x 10-4	30
	27.3	69.1	8.68 x 10-4	30
	31.6	69.7	6.45 x 10-4	40
	38.8	67.3	6.17 x 10-4	40
	32.5	67.3	5.35 x 10-4	50
	36.1	69.8	4.19 x 10-4	60
	32.6	68.9	4.16 x 10-4	60
	41.2	68.6	3.38 x 10-4	70
	32.5	64.2	3.13 x 10-4	80
	30.8	71.2	3.12 x 10-4	80
	33.5	69.9	3.04 x 10-4	80
	34.8	70.9	2.75 x 10-4	90
	32.5	69.7	2.35 x 10-4	100
	32.7	65.9	2.25 x 10-4	100
S002-0	20.5	73.4	2.06 x 10-3	0
	28.3	68.4	1.32 x 10-3	5
	32.2	65.1	8.01 x 10-4	10
	40.1	63.1	4.29 x 10-4	20
	37.8	64.0	4.33 x 10-4	20
	94.6	10.1	2.85 x 10-4	30
	160.6	5.8	2.66 x 10-4	30
	44.4	60.7	1.62 x 10-4	50
	42.4	60.8	1.54 x 10-4	50
	46.6	61.1	1.32 x 10-4	60
	46.0	57.6	1.26 x 10-4	60
	49.4	59.9	1.09 x 10-4	70
	54.1	62.7	1.08 x 10-4	70
	52.5	55.3	8.75 x 10-5	80
	53.3	58.7	8.45 x 10-5	80
S003-1	72.8	69.7	1.43 x 10-3	0
	64.4	64.2	1.08 x 10-3	10
	51.8	61.8	6.96 x 10-4	30
	50.8	61.7	6.73 x 10-4	30
	49.0	62.3	4.66 x 10-4	50
	47.1	60.4	4.53 x 10-4	50
	48.2	62.3	3.08 x 10-4	70
	49.5	60.7	2.89 x 10-4	70
	48.6	60.6	2.58 x 10-4	80
	45.6	59.9	2.44 x 10-4	80
S004-0	70.2	80.7	1.86 x 10-3	0
	68.7	65.3	7.30 x 10-4	20
	61.6	65.1	2.85 x 10-4	50
	65.1	63.0	1.78 x 10-4	70
	62.2	62.0	1.69 x 10-4	70
	61.5	60.7	1.54 x 10-4	80
	62.7	61.9	1.55 x 10-4	80
S005-1	80.9	78.7	1.86 x 10-3	0
	65.9	66.5	9.14 x 10-4	20
	64.6	63.7	3.61 x 10-4	50

Sample	Declination	Inclination	Intensity (emu/cc)	Demagnetization (mT)
	66.8	60.9	2.32 x 10-4	70
	67.1	63.0	1.95 x 10-4	80
	64.6	61.7	1.82 x 10-4	80
S006-0	52.5	71.0	2.59 x 10-3	0
	60.2	65.4	1.66 x 10-3	20
	63.2	62.2	6.77 x 10-4	50
	65.0	62.3	3.54 x 10-4	80
	64.4	62.1	3.34 x 10-4	80
S007-0	36.2	68.6	3.38 x 10-3	0
	61.5	63.0	1.17 x 10-3	20
	66.4	59.5	7.99 x 10-4	50
	67.1	60.3	6.46 x 10-4	80
	65.5	60.2	6.44 x 10-4	80
S008-0*	9.8	54.2	1.22 x 10-3	0
	293.7	46.1	1.11 x 10-4	10
	224.3	-25.9	4.43 x 10-5	20
	223.6	-27.9	4.67 x 10-5	20
	208.1	-39.1	3.52 x 10-5	30
	210.8	-49.7	3.63 x 10-5	40
	205.7	-52.1	3.31 x 10-5	40
	212.6	-48.7	3.31 x 10-5	50
	205.5	-56.0	3.07 x 10-5	50
	199.8	-53.8	2.73 x 10-5	70
	203.8	-51.5	2.17 x 10-5	70
	191.8	-44.8	1.79 x 10-5	100
	231.0	-61.4	1.78 x 10-5	100
S009-1	272.4	69.9	8.75 x 10-4	0
	215.5	-23.9	9.41 x 10-5	20
	206.2	-39.9	4.12 x 10-5	40
	198.9	-41.3	3.69 x 10-5	40
	208.0	-45.2	3.01 x 10-5	50
	191.1	-53.7	2.68 x 10-5	50
	212.3	-39.0	3.45 x 10-5	60
	199.5	-47.3	2.08 x 10-5	60
S010-1	311.7	15.2	8.36 x 10-4	0
	254.8	-8.9	1.30 x 10-4	10
	226.4	-31.7	6.02 x 10-5	20
	216.6	-48.7	2.99 x 10-5	40
	194.3	-49.8	2.55 x 10-5	40
	210.0	-47.5	2.65 x 10-5	50
	209.2	-46.6	2.39 x 10-5	50
S011-1	274.7	55.7	8.98 x 10-4	0
	241.4	5.4	1.29 x 10-4	10
	220.9	-27.6	6.47 x 10-5	20
	202.0	-46.1	2.55 x 10-5	40
	209.3	-45.8	2.58 x 10-5	40
S012-1	300.6	37.0	8.52 x 10-4	0
	248.4	-36.6	1.54 x 10-4	10
	211.5	-26.3	2.16 x 10-4	20
	209.4	-36.2	7.84 x 10-5	40
	209.4	-33.0	6.54 x 10-5	40
S013-1	14.5	27.8	9.29 x 10-4	0
	219.0	-39.1	3.68 x 10-5	20
	207.3	-50.0	2.80 x 10-5	40
	197.0	-50.2	2.66 x 10-5	40
S014-1	8.0	43.4	1.01 x 10-3	0
	231.4	-40.6	3.30 x 10-5	20
	214.2	-53.4	2.61 x 10-5	40
	222.7	-55.5	3.01 x 10-5	40
S015-1*	228.0	51.4	7.07 x 10-4	0
	205.0	-17.4	1.64 x 10-4	10

Sample	Declination	Inclination	Intensity (emu/cc)	Demagnetization (mT)
	198.0	-37.1	9.09 x 10-5	20
	198.3	-39.4	8.87 x 10-5	20
	206.9	-47.2	5.74 x 10-5	30
	202.0	-46.2	5.47 x 10-5	30
	210.6	-46.0	3.74 x 10-5	40
	210.6	-40.2	3.97 x 10-5	40
	208.6	-44.3	3.39 x 10-5	50
	198.7	-44.0	2.77 x 10-5	50
	207.6	-47.1	1.88 x 10-5	60
	231.8	-44.6	1.38 x 10-5	60
	183.3	-46.4	1.45 x 10-5	80
	212.7	-29.0	1.39 x 10-5	80
	173.1	-72.3	8.50 x 10-6	100
	194.7	-13.1	1.22 x 10-5	100
S016-1	238.5	73.2	7.23 x 10-4	0
	193.7	2.2	1.19 x 10-4	10
	191.6	-37.1	8.15 x 10-5	20
	188.8	-39.2	5.67 x 10-5	30
	193.5	-41.4	5.71 x 10-5	30
	192.9	-47.2	4.27 x 10-5	40
	193.2	-47.0	4.30 x 10-5	40
	187.0	-45.6	3.74 x 10-5	50
	196.4	-52.2	3.37 x 10-5	50
S017-0	205.3	-54.0	9.51 x 10-4	0
	197.5	-53.1	8.75 x 10-4	20
	199.4	-52.3	4.86 x 10-4	40
	195.4	-53.6	4.63 x 10-4	40
S018-0	16.5	55.2	6.80 x 10-4	0
	203.0	-41.4	6.28 x 10-5	20
	197.9	-48.9	3.84 x 10-5	40
	191.6	-47.7	3.30 x 10-5	40
S019-1	312.6	31.7	6.71 x 10-4	0
	224.0	-40.8	4.08 x 10-5	20
	208.8	-46.8	1.85 x 10-5	40
	199.2	-49.8	1.57 x 10-5	40
S020-1	347.4	45.7	4.50 x 10-4	0
	197.1	-54.9	9.25 x 10-5	20
	187.4	-49.5	4.32 x 10-5	40
	184.9	-46.8	4.07 x 10-5	40
S021-1	191.2	-32.2	3.98 x 10-4	0
	194.2	-49.7	6.35 x 10-4	20
	198.5	-48.6	2.48 x 10-4	40
	196.7	-49.7	2.57 x 10-4	40
	192.2	-50.4	2.54 x 10-4	40
	192.8	-51.1	2.56 x 10-4	40
S022-1*	23.0	43.4	1.60 x 10-3	0
	249.2	-67.7	2.11 x 10-4	10
	217.3	-59.7	2.15 x 10-4	20
	212.6	-61.2	2.33 x 10-4	20
	202.9	-58.9	1.73 x 10-4	30
	207.8	-61.8	1.25 x 10-4	40
	202.6	-59.9	1.13 x 10-4	40
	223.1	-60.0	9.31 x 10-5	50
	210.5	-56.8	8.48 x 10-5	50
	209.7	-55.7	5.78 x 10-5	60
	198.8	-50.7	6.35 x 10-5	60
	191.0	-41.7	3.60 x 10-5	80
	175.5	-30.5	3.23 x 10-5	80
	246.0	-61.0	5.40 x 10-5	80
S024-1	7.5	58.8	1.52 x 10-3	0
	218.6	-62.4	1.51 x 10-4	20

Sample	Declination	Inclination	Intensity (emu/cc)	Demagnetization (mT)
	224.4	-53.3	7.44 x 10-5	40
	203.2	-60.3	6.39 x 10-5	40
	205.6	-53.0	4.31 x 10-5	50
	224.4	-63.6	4.80 x 10-5	50
S025-1	79.6	31.3	2.10 x 10-3	0
	166.7	-66.8	1.65 x 10-4	20
	168.7	-66.4	1.68 x 10-4	20
	190.1	-67.3	1.38 x 10-4	30
	198.7	-57.2	1.01 x 10-4	40
	199.5	-57.4	1.01 x 10-4	40
	212.4	-55.6	7.51 x 10-5	50
	200.4	-66.3	6.35 x 10-5	50
	221.8	-62.4	4.92 x 10-5	60
	195.6	-59.0	4.99 x 10-5	60
S026-1	319.0	26.2	1.94 x 10-3	0
	226.5	-52.7	1.25 x 10-4	20
	220.9	-63.5	4.54 x 10-5	50
	220.1	-51.3	4.82 x 10-5	50
S027-1	210.2	-69.3	4.66 x 10-3	0
	192.7	-71.2	4.19 x 10-3	20
	195.2	-69.8	1.19 x 10-3	50
	191.7	-70.5	1.11 x 10-3	50
S028-1*	60.2	65.1	1.02 x 10-3	0
	54.2	67.7	7.07 x 10-4	10
	54.3	71.7	3.81 x 10-4	20
	55.1	71.4	3.54 x 10-4	20
	43.4	73.7	2.12 x 10-4	30
	50.2	79.0	1.11 x 10-4	40
	75.1	73.3	1.25 x 10-4	40
	19.8	71.6	6.52 x 10-5	50
	243.7	80.3	3.95 x 10-5	50
	349.1	52.8	4.00 x 10-5	60
	239.5	-4.8	2.38 x 10-5	60
	339.4	2.5	4.68 x 10-5	80
	249.5	-42.9	5.01 x 10-5	80
	342.3	-23.5	5.10 x 10-5	100
	341.5	-24.8	5.13 x 10-5	100
S029-0	39.6	75.8	8.29 x 10-4	0
	26.1	78.3	5.03 x 10-4	10
	18.4	85.3	2.30 x 10-4	20
	356.7	84.8	2.18 x 10-4	20
	333.7	78.7	1.25 x 10-4	30
	353.4	80.4	1.25 x 10-4	30
	26.0	84.5	9.33 x 10-5	40
S030-2	348.2	62.7	9.00 x 10-4	0
	351.6	65.2	5.13 x 10-4	10
	351.6	68.4	2.69 x 10-4	20
	352.3	69.4	1.78 x 10-4	30
	347.6	71.4	1.07 x 10-4	40
	339.3	70.5	7.08 x 10-5	50
	329.8	62.6	4.87 x 10-5	60
	317.7	55.7	3.69 x 10-5	70
	318.1	45.6	3.03 x 10-5	80
S031-1	335.5	78.1	1.02 x 10-3	0
	333.8	79.4	6.66 x 10-4	10
	324.3	81.2	3.63 x 10-4	20
	325.2	80.1	3.51 x 10-4	20
S032-3	339.1	71.7	6.12 x 10-4	0
	337.3	76.7	3.90 x 10-4	10
	325.5	82.0	1.91 x 10-4	20
	304.8	83.4	1.16 x 10-4	30

Sample	Declination	Inclination	Intensity (emu/cc)	Demagnetization (mT)
	302.6	82.5	7.44 x 10-5	40
	304.3	78.9	4.97 x 10-5	50
	303.7	72.6	3.67 x 10-5	60
S033-1	308.2	65.7	6.20 x 10-4	0
	304.8	65.6	3.50 x 10-4	10
	303.2	66.0	1.82 x 10-4	20
	304.3	66.3	1.04 x 10-4	30
	306.4	65.6	6.35 x 10-5	40
	311.8	61.9	4.15 x 10-5	50
	308.3	53.6	2.91 x 10-5	60
S034-1*	104.4	62.0	8.44 x 10-4	0
	66.2	71.4	3.39 x 10-4	10
	52.9	72.2	1.69 x 10-4	20
	51.3	72.2	1.58 x 10-4	20
	44.8	70.4	9.16 x 10-5	30
	46.9	70.8	8.31 x 10-5	30
	37.6	73.2	4.78 x 10-5	40
	46.3	71.0	4.28 x 10-5	40
	34.7	71.8	2.90 x 10-5	50
	39.7	69.2	2.62 x 10-5	50
	13.6	72.0	1.92 x 10-5	60
	20.2	74.1	1.78 x 10-5	60
	6.6	74.8	1.34 x 10-5	80
	335.2	71.0	1.12 x 10-5	80
	350.4	59.7	1.30 x 10-5	100
	21.3	79.4	8.72 x 10-6	100
S035-1	96.2	66.1	8.28 x 10-4	0
	54.7	77.4	4.79 x 10-4	10
	35.0	77.0	2.83 x 10-4	20
	30.0	77.7	2.69 x 10-4	20
	21.9	75.9	1.69 x 10-4	30
	23.0	75.6	1.58 x 10-4	30
	9.9	75.0	9.58 x 10-5	40
	22.9	78.3	8.92 x 10-5	40
S036-1	39.1	46.8	8.86 x 10-4	0
	26.8	66.6	2.22 x 10-4	20
	24.2	68.8	1.99 x 10-4	20
	17.8	67.4	1.18 x 10-4	30
	18.3	65.5	1.07 x 10-4	30
	9.3	67.4	6.58 x 10-5	40
	13.4	69.4	6.09 x 10-5	40
S037-1	76.2	60.7	8.11 x 10-4	0
	37.0	69.0	6.90 x 10-5	30
	36.7	69.0	6.91 x 10-5	30
	27.8	67.9	3.68 x 10-5	40
	50.7	67.3	3.22 x 10-5	40
S038-1	129.1	73.1	8.56 x 10-4	0
	34.4	78.3	1.99 x 10-4	20
	34.4	77.9	1.96 x 10-4	20
	351.7	58.0	7.80 x 10-6	100
	327.3	55.9	6.53 x 10-6	100
S039-1	105.3	2.4	2.73 x 10-3	0
	106.5	0.7	2.74 x 10-3	10
	108.5	-2.2	2.68 x 10-3	20
	110.7	-4.3	2.49 x 10-3	30
	111.1	-2.2	2.09 x 10-3	40
	111.8	-0.8	2.00 x 10-3	40
	109.5	3.5	1.51 x 10-3	60
	108.6	7.4	1.43 x 10-3	60
	108.1	5.9	1.23 x 10-3	80
	108.7	6.9	1.18 x 10-3	80

Sample	Declination	Inclination	Intensity (emu/cc)	Demagnetization (mT)
	106.0	6.7	1.06 x 10-3	100
	107.1	8.3	1.01 x 10-3	100
S046-2*	229.8	41.7	1.16 x 10-3	0
	204.8	-27.5	3.82 x 10-4	10
	203.1	-54.6	2.49 x 10-4	20
	205.4	-56.7	2.42 x 10-4	20
	200.3	-60.6	1.70 x 10-4	30
	199.2	-61.6	1.26 x 10-4	40
	203.0	-59.5	1.15 x 10-4	40
	199.4	-60.5	7.10 x 10-5	60
	194.1	-56.2	6.39 x 10-5	60
	192.3	-60.4	5.32 x 10-5	80
	208.5	-56.6	4.78 x 10-5	80
	203.2	-62.6	4.56 x 10-5	100
	218.1	-60.0	3.72 x 10-5	100
S047-0	153.9	10.7	1.15 x 10-3	0
	191.4	-57.3	2.57 x 10-4	20
	194.5	-59.2	1.65 x 10-4	30
	195.9	-58.7	1.54 x 10-4	30
	196.8	-56.5	1.06 x 10-4	40
	193.8	-57.9	1.01 x 10-4	40
	194.5	-59.2	6.22 x 10-5	60
	196.0	-52.5	5.48 x 10-5	60
S048-1	123.4	53.5	1.00 x 10-3	0
	185.5	-56.4	1.46 x 10-4	30
	188.2	-57.6	1.45 x 10-4	30
	186.8	-57.7	1.15 x 10-4	40
	193.0	-57.3	1.11 x 10-4	40
	185.0	-58.0	8.48 x 10-5	60
	188.7	-58.4	7.82 x 10-5	60
	201.5	-57.1	7.01 x 10-5	80
	189.6	-61.6	6.58 x 10-5	80
	199.5	-60.9	6.51 x 10-5	100
	194.9	-62.0	5.67 x 10-5	100
S049-1	86.1	52.4	9.01 x 10-4	0
	177.6	-53.3	1.27 x 10-4	30
	180.4	-52.2	1.24 x 10-4	30
	176.7	-54.1	9.78 x 10-5	40
	180.9	-56.0	8.92 x 10-5	40
	187.4	-56.3	7.45 x 10-5	60
	180.5	-56.9	6.56 x 10-5	60
	180.9	-58.9	6.98 x 10-5	80
	185.9	-57.5	5.96 x 10-5	80
S050-1	149.3	31.7	8.16 x 10-4	0
	188.0	-47.2	2.60 x 10-4	30
	189.9	-48.0	2.58 x 10-4	30
	190.1	-48.2	2.09 x 10-4	40
	192.9	-49.5	1.94 x 10-4	40
	192.6	-51.7	1.56 x 10-4	60
	194.0	-53.8	1.40 x 10-4	60
	197.3	-49.4	1.15 x 10-4	80
	194.1	-51.1	1.09 x 10-4	80
	195.0	-52.4	9.38 x 10-5	100
	193.3	-52.5	8.25 x 10-5	100
S051-1	126.2	-18.3	7.30 x 10-4	0
	194.0	-54.4	1.99 x 10-4	30
	190.5	-53.9	1.32 x 10-4	40
	193.6	-53.3	1.21 x 10-4	40
	192.8	-60.3	7.38 x 10-5	60
	200.8	-45.3	5.75 x 10-5	60
	194.5	-67.8	4.86 x 10-5	80

Sample	Declination	Inclination	Intensity (emu/cc)	Demagnetization (mT)
	202.1	-53.8	3.39 x 10-5	80
S052-1*	66.8	78.6	4.75 x 10-3	0
	66.6	78.1	3.44 x 10-3	10
	59.5	78.6	2.18 x 10-3	20
	58.9	78.8	2.08 x 10-3	20
	54.0	78.7	1.19 x 10-3	30
	60.8	78.5	6.42 x 10-4	40
	62.0	77.8	5.82 x 10-4	40
	67.2	78.4	2.90 x 10-4	60
	77.8	78.5	2.75 x 10-4	60
	75.4	75.1	2.03 x 10-4	80
	77.5	76.7	2.08 x 10-4	80
	84.4	76.4	2.11 x 10-4	80
S053-1	49.2	71.0	4.57 x 10-3	0
	49.5	77.3	2.94 x 10-3	10
	50.5	77.9	1.83 x 10-3	20
	50.4	77.9	1.75 x 10-3	20
	48.3	77.2	9.87 x 10-4	30
	43.2	77.6	9.30 x 10-4	30
	39.0	78.6	4.93 x 10-4	40
	63.0	77.6	4.42 x 10-4	40
S054-1	38.0	46.1	1.50 x 10-3	0
	64.3	71.5	4.73 x 10-4	10
	68.3	73.7	2.69 x 10-4	20
	71.8	75.1	2.48 x 10-4	20
	67.9	74.2	1.77 x 10-4	30
	69.1	74.0	1.57 x 10-4	30
S055-1	44.5	75.2	5.12 x 10-3	0
	60.9	75.8	4.77 x 10-3	10
	60.0	76.1	3.81 x 10-3	20
	59.3	76.2	3.72 x 10-3	20
	57.5	76.6	2.49 x 10-3	30
	58.5	76.4	2.35 x 10-3	30
S056-2	7.8	70.0	3.38 x 10-3	0
	40.2	75.0	2.07 x 10-3	10
	46.5	76.0	1.41 x 10-3	20
	52.0	76.0	1.36 x 10-3	20
	49.0	75.7	9.23 x 10-4	30
	52.8	75.4	8.77 x 10-4	30
S057-1	48.8	67.2	3.68 x 10-3	0
	59.6	73.9	2.99 x 10-3	10
	56.0	74.0	2.12 x 10-3	20
	56.6	74.3	2.06 x 10-3	20
	53.3	74.3	1.30 x 10-3	30
	55.5	73.4	1.22 x 10-3	30
S058-1*	40.0	68.0	3.18 x 10-3	0
	275.3	82.1	2.10 x 10-3	10
	261.3	80.1	1.57 x 10-3	15
	251.9	77.8	1.03 x 10-3	20
	250.1	76.3	7.08 x 10-4	25
	239.0	72.2	4.94 x 10-4	30
	238.5	71.9	4.57 x 10-4	30
	233.5	68.4	3.31 x 10-4	35
	230.8	65.9	3.36 x 10-4	35
	224.8	62.2	2.44 x 10-4	40
	218.3	43.2	1.37 x 10-4	50
	207.6	15.8	9.41 x 10-5	60
	202.9	-3.3	7.39 x 10-5	70
S059-1	15.1	47.6	2.86 x 10-3	0
	334.7	73.8	7.01 x 10-4	10
	320.9	73.6	4.29 x 10-4	15

Sample	Declination	Inclination	Intensity (emu/cc)	Demagnetization (mT)
	319.8	76.0	3.04 x 10-4	20
	313.7	76.0	2.07 x 10-4	25
	307.7	77.5	1.46 x 10-4	30
	286.5	75.2	8.09 x 10-5	40
	267.9	72.8	4.00 x 10-5	50
S060-1	49.0	66.2	2.05 x 10-3	0
	270.1	83.3	4.84 x 10-4	10
	270.2	82.5	3.55 x 10-4	15
	250.0	79.5	3.02 x 10-4	20
	254.3	79.9	2.63 x 10-4	25
	266.8	81.9	2.32 x 10-4	30
	244.8	82.4	1.63 x 10-4	40
	225.2	79.5	1.18 x 10-4	50
	209.4	80.4	8.77 x 10-5	60
S061-1	307.5	46.0	1.11 x 10-3	0
	267.0	62.3	2.01 x 10-4	10
	257.2	67.6	1.47 x 10-4	15
	258.1	70.5	1.19 x 10-4	20
	260.6	72.5	1.03 x 10-4	25
	258.6	73.2	7.93 x 10-5	30
	245.1	72.9	4.85 x 10-5	40
	261.8	61.4	3.07 x 10-5	50
	241.1	64.7	2.88 x 10-5	50
	231.4	54.1	1.80 x 10-5	60
	243.5	70.1	1.96 x 10-5	60
S062-1	62.1	2.7	1.23 x 10-3	0
	71.6	51.6	9.02 x 10-5	10
	78.0	81.3	7.96 x 10-5	15
	242.2	89.7	7.31 x 10-5	20
	218.3	79.9	6.14 x 10-5	30
	268.3	77.4	3.40 x 10-5	40
	234.9	67.3	2.86 x 10-5	45
	269.9	79.4	3.13 x 10-5	45
S063-1	16.3	-7.3	9.49 x 10-4	0
	350.1	60.6	7.80 x 10-5	10
	333.9	76.6	8.24 x 10-5	15
	314.9	80.6	8.31 x 10-5	20
	282.1	82.1	8.02 x 10-5	25
	267.8	80.7	6.66 x 10-5	30
	268.1	77.1	5.42 x 10-5	35
	254.4	79.4	4.09 x 10-5	40
	258.8	76.0	4.35 x 10-5	40
	275.5	80.0	3.25 x 10-5	45
	219.5	83.0	3.04 x 10-5	50
	253.1	80.0	2.82 x 10-5	50
	308.8	84.7	2.74 x 10-5	50
S064-1	347.3	36.2	1.80 x 10-3	0
	322.4	58.4	2.76 x 10-4	10
	311.1	67.8	1.86 x 10-4	15
	311.2	73.0	1.45 x 10-4	20
	298.0	77.3	1.10 x 10-4	25
	280.7	74.0	8.43 x 10-5	30
	274.3	79.0	6.62 x 10-5	35
	295.4	74.1	5.27 x 10-5	40
	270.1	72.2	3.79 x 10-5	45
	282.6	77.8	3.33 x 10-5	50
	236.1	65.2	2.07 x 10-5	55
	194.9	72.6	2.61 x 10-5	55
	250.3	65.2	1.71 x 10-5	60
	193.6	68.7	1.54 x 10-5	65
	95.7	81.5	9.27 x 10-6	70

Sample	Declination	Inclination	Intensity (emu/cc)	Demagnetization (mT)
	269.4	70.2	4.12 x 10-6	70
S065-1	62.7	61.3	2.17 x 10-3	0
	62.2	78.3	3.53 x 10-4	10
	50.0	81.7	2.21 x 10-4	15
	2.5	85.6	1.69 x 10-4	20
	299.8	89.1	1.24 x 10-4	25
	251.3	87.7	1.02 x 10-4	30
	283.4	82.7	8.05 x 10-5	35
	271.2	83.5	6.55 x 10-5	40
	272.8	87.1	5.13 x 10-5	45
	261.0	86.1	3.36 x 10-5	50
S066-1*	84.7	67.6	3.65 x 10-3	0
	49.1	75.8	2.24 x 10-3	10
	46.5	75.9	1.62 x 10-3	15
	45.6	77.2	1.23 x 10-3	20
	45.8	76.8	1.02 x 10-3	25
	44.3	78.0	8.84 x 10-4	30
	48.0	78.1	7.68 x 10-4	40
	42.8	79.2	6.14 x 10-4	60
	45.0	75.9	5.40 x 10-4	75
S067-1	95.9	53.9	2.52 x 10-3	0
	59.6	75.3	1.30 x 10-3	10
	51.8	76.3	9.76 x 10-4	15
	51.5	76.6	7.72 x 10-4	20
	47.1	77.7	4.98 x 10-4	30
S068-1	53.4	68.3	3.49 x 10-3	0
	61.1	86.5	1.96 x 10-3	10
	61.6	87.2	1.59 x 10-3	15
	63.2	86.9	1.36 x 10-3	20
	73.0	87.8	1.11 x 10-3	30
	72.2	87.3	1.10 x 10-3	30
	76.1	87.7	9.47 x 10-4	40
	80.0	87.6	8.26 x 10-4	50
S069-1	78.3	69.3	3.78 x 10-3	0
	51.2	79.1	1.97 x 10-3	10
	48.8	79.5	1.64 x 10-3	15
	49.1	80.3	1.41 x 10-3	20
	46.7	81.0	1.22 x 10-3	30
	45.6	81.7	1.06 x 10-3	40
S070-1	101.9	58.9	4.11 x 10-3	0
	65.1	75.4	2.29 x 10-3	10
	60.4	75.7	1.76 x 10-3	15
	59.3	76.4	1.46 x 10-3	20
	61.5	76.7	1.22 x 10-3	30
	59.5	76.7	1.05 x 10-3	40
S071-1	73.1	58.2	3.44 x 10-3	0
	61.7	79.3	1.83 x 10-3	10
	58.5	80.3	1.50 x 10-3	15
	55.7	80.4	1.28 x 10-3	20
	50.4	81.3	1.02 x 10-3	30
	54.6	81.2	8.82 x 10-4	40
S072-1*	82.2	-45.4	8.89 x 10-4	0
	174.1	-69.9	9.35 x 10-4	10
	182.1	-68.3	8.92 x 10-4	15
	185.1	-67.4	7.87 x 10-4	20
	188.7	-66.3	5.34 x 10-4	30
	194.0	-66.3	2.97 x 10-4	40
	196.1	-66.5	1.86 x 10-4	50
	188.1	-65.9	1.11 x 10-4	60
	194.2	-65.0	1.12 x 10-4	60
S073-1	61.3	53.3	1.46 x 10-3	0

Sample	Declination	Inclination	Intensity (emu/cc)	Demagnetization (mT)
	121.5	37.3	5.92 x 10-5	10
	169.1	-50.0	9.92 x 10-5	15
	169.2	-54.7	1.11 x 10-4	20
	169.4	-58.5	9.95 x 10-5	30
	174.1	-64.7	8.59 x 10-5	40
	176.9	-62.0	6.67 x 10-5	50
	171.9	-63.0	6.96 x 10-5	50
	167.9	-61.9	6.47 x 10-5	55
	174.4	-57.8	6.67 x 10-5	60
	163.9	-64.4	6.71 x 10-5	60
	171.2	-60.9	5.79 x 10-5	70
	166.0	-59.9	5.68 x 10-5	70
	183.8	-51.6	5.71 x 10-5	75
	167.2	-55.5	6.02 x 10-5	75
S074-1	92.5	19.3	9.86 x 10-4	0
	130.0	-48.5	3.10 x 10-4	10
	162.8	-63.1	3.65 x 10-4	15
	174.8	-64.2	3.61 x 10-4	20
	180.8	-64.9	3.22 x 10-4	25
	191.8	-65.1	2.85 x 10-4	30
	185.3	-64.9	2.64 x 10-4	30
	186.7	-63.7	2.15 x 10-4	35
	190.1	-63.1	1.76 x 10-4	40
	189.9	-61.8	1.13 x 10-4	50
	189.6	-66.3	8.05 x 10-5	60
	192.5	-64.1	7.75 x 10-5	60
S075-1	68.6	37.7	1.37 x 10-3	0
	94.9	22.0	9.69 x 10-5	10
	155.6	-52.2	1.05 x 10-4	15
	179.7	-62.0	1.15 x 10-4	20
	188.0	-60.6	1.04 x 10-4	30
	186.6	-62.2	9.11 x 10-5	40
	193.9	-61.1	6.83 x 10-5	50
	189.9	-59.9	7.29 x 10-5	50
	175.7	-64.8	7.26 x 10-5	50
S076-1	66.1	55.5	9.28 x 10-4	0
	161.8	-36.1	9.37 x 10-5	10
	185.6	-55.5	1.40 x 10-4	20
	190.5	-60.3	1.12 x 10-4	30
	189.6	-61.3	1.01 x 10-4	35
	192.4	-57.7	8.76 x 10-5	40
	179.5	-62.6	7.69 x 10-5	45
	186.9	-57.3	7.76 x 10-5	45
S077-1	164.0	-47.6	1.50 x 10-3	0
	179.8	-64.4	1.55 x 10-3	10
	183.7	-65.9	1.48 x 10-3	15
	184.4	-66.7	1.31 x 10-3	20
	185.4	-66.7	1.10 x 10-3	25
	183.9	-66.7	8.82 x 10-4	30
	184.6	-67.0	6.72 x 10-4	35
S078-1	172.8	-80.5	1.77 x 10-3	0
	184.5	-78.4	1.94 x 10-3	10
	185.1	-78.2	1.90 x 10-3	15
	185.9	-77.0	1.79 x 10-3	20
	186.9	-76.5	1.61 x 10-3	25
	185.4	-77.1	1.39 x 10-3	30
	187.4	-76.6	1.22 x 10-3	35
S085-1*	57.6	-51.3	6.27 x 10-4	0
	46.0	-79.7	4.85 x 10-4	10
	47.2	-83.9	3.94 x 10-4	15
	50.4	-81.9	2.86 x 10-4	20

Sample	Declination	Inclination	Intensity (emu/cc)	Demagnetization (mT)
	55.8	-80.8	2.74 x 10-4	25
	63.4	-85.3	1.69 x 10-4	30
	59.0	-85.1	1.59 x 10-4	30
	76.1	-86.4	1.31 x 10-4	35
	77.6	-87.9	1.06 x 10-4	40
	90.3	-87.7	8.75 x 10-5	45
	78.7	-87.4	6.27 x 10-5	55
	166.7	-84.8	4.84 x 10-5	65
	208.0	-86.7	4.71 x 10-5	65
S086-1	76.1	-74.9	1.18 x 10-3	0
	118.0	-85.7	1.29 x 10-3	10
	147.8	-86.2	1.20 x 10-3	15
	146.5	-86.2	1.03 x 10-3	20
	171.3	-85.5	6.56 x 10-4	30
	174.4	-85.7	4.01 x 10-4	40
	179.7	-85.6	2.60 x 10-4	50
	187.9	-86.1	2.01 x 10-4	60
	191.7	-84.5	1.96 x 10-4	60
S087-1	54.0	-46.5	7.37 x 10-4	0
	58.3	-80.7	6.93 x 10-4	10
	149.9	-86.9	6.06 x 10-4	20
	139.5	-86.6	4.53 x 10-4	30
	100.3	-85.9	4.42 x 10-4	30
	128.1	-86.1	3.74 x 10-4	35
	132.7	-86.8	2.49 x 10-4	45
	177.4	-85.9	1.85 x 10-4	55
	171.2	-85.1	1.87 x 10-4	55
	174.2	-85.1	1.51 x 10-4	65
	162.2	-85.9	1.34 x 10-4	75
S088-1	65.5	35.3	5.19 x 10-4	0
	70.3	-80.9	4.10 x 10-4	10
	99.6	-86.3	3.06 x 10-4	20
	168.3	-87.6	1.97 x 10-4	30
	129.6	-88.9	1.90 x 10-4	30
	136.6	-87.4	1.30 x 10-4	40
	170.0	-85.9	8.80 x 10-5	50
	139.7	-88.8	7.71 x 10-5	60
S089-1	350.6	-54.7	7.37 x 10-4	0
	14.7	-86.6	7.37 x 10-4	10
	98.2	-87.9	5.23 x 10-4	20
	96.6	-87.7	3.40 x 10-4	30
	133.3	-84.7	2.10 x 10-4	40
	136.0	-84.6	1.43 x 10-4	50
	154.2	-83.3	1.15 x 10-4	60
	137.3	-83.1	1.15 x 10-4	60
	135.9	-84.9	9.76 x 10-5	75
S090-1	80.8	-63.3	1.08 x 10-3	0
	103.0	-81.9	1.06 x 10-3	10
	117.3	-83.1	8.00 x 10-4	20
	125.7	-84.1	5.08 x 10-4	30
	124.9	-83.9	2.98 x 10-4	40
	162.5	-84.3	1.96 x 10-4	50
	153.3	-85.0	1.52 x 10-4	60
	163.6	-83.7	1.27 x 10-4	70
S091-1	82.2	17.1	1.99 x 10-4	0
	129.7	-84.2	1.46 x 10-4	20
	143.8	-84.3	9.36 x 10-5	30
	126.6	-82.3	7.19 x 10-5	40
	167.1	-85.9	5.13 x 10-5	50
	211.5	-82.1	3.74 x 10-5	60
	187.7	-83.2	3.85 x 10-5	60

Sample	Declination	Inclination	Intensity (emu/cc)	Demagnetization (mT)
	209.2	-66.1	2.84 x 10-5	70
	182.4	-79.0	2.54 x 10-5	70
S092-1*	33.6	25.6	5.83 x 10-4	0
	24.3	-45.0	1.34 x 10-4	10
	25.9	-66.3	1.19 x 10-4	15
	22.4	-74.5	9.32 x 10-5	20
	18.2	-76.3	7.19 x 10-5	25
	12.4	-79.5	5.93 x 10-5	30
	12.6	-80.6	6.06 x 10-5	30
	30.0	-83.1	5.07 x 10-5	35
	49.8	-83.2	4.26 x 10-5	40
	2.1	-77.2	3.93 x 10-5	45
	123.4	-89.6	3.75 x 10-5	45
	285.4	-87.9	3.02 x 10-5	55
	88.5	-85.5	2.41 x 10-5	65
	47.4	-80.9	2.46 x 10-5	75
S093-1	57.1	-83.5	1.46 x 10-3	0
	66.0	-87.3	1.51 x 10-3	5
	81.8	-87.9	1.53 x 10-3	10
	70.0	-87.4	1.49 x 10-3	15
	63.9	-87.2	1.40 x 10-3	20
	144.9	-88.7	1.66 x 10-3	30
	169.2	-88.1	8.74 x 10-4	40
	165.7	-87.7	6.34 x 10-4	50
	59.8	-87.0	4.54 x 10-4	60
S094-1	50.2	-82.8	1.45 x 10-3	0
	57.3	-84.8	1.40 x 10-3	5
	61.1	-85.3	1.41 x 10-3	10
	68.2	-85.7	1.19 x 10-3	20
	83.3	-86.3	8.73 x 10-4	30
	117.4	-87.2	5.97 x 10-4	40
	54.4	-85.2	3.73 x 10-4	50
	68.9	-86.3	3.65 x 10-4	50
S095-1	37.1	-81.9	1.97 x 10-3	0
	62.8	-86.7	1.88 x 10-3	5
	62.8	-86.4	1.84 x 10-3	10
	91.5	-87.4	1.42 x 10-3	20
	82.0	-86.6	9.04 x 10-4	30
	120.2	-88.4	5.74 x 10-4	40
	113.7	-88.6	4.08 x 10-4	50
S096-1	48.2	11.1	4.49 x 10-4	0
	43.5	-67.7	1.38 x 10-4	5
	46.6	-69.6	1.34 x 10-4	10
	51.2	-76.5	8.80 x 10-5	15
	80.7	-82.0	5.83 x 10-5	20
	74.4	-80.0	4.05 x 10-5	30
	65.0	-79.5	3.07 x 10-5	40
	126.9	-80.5	2.45 x 10-5	50
	163.7	-87.0	2.59 x 10-5	60
S097-1	343.3	37.0	4.57 x 10-4	0
	359.3	-69.0	1.07 x 10-4	5
	5.1	-72.2	1.07 x 10-4	10
	359.5	-80.5	4.80 x 10-5	20
	224.9	-88.7	3.30 x 10-5	30
	91.6	-82.0	2.35 x 10-5	45
	15.2	-53.2	1.58 x 10-5	55
	159.7	-81.8	1.58 x 10-5	55
	358.5	-81.2	2.03 x 10-5	55
S104-1*	12.9	66.0	6.94 x 10-3	0
	13.0	66.5	5.31 x 10-3	5
	13.4	66.7	5.21 x 10-3	10

Sample	Declination	Inclination	Intensity (emu/cc)	Demagnetization (mT)
	13.4	66.5	4.73 x 10-3	15
	15.9	67.2	3.93 x 10-3	20
	14.6	67.0	3.21 x 10-3	25
	15.6	67.2	2.51 x 10-3	30
	13.4	67.4	1.59 x 10-3	40
	17.4	67.8	7.59 x 10-4	60
	17.6	68.2	6.24 x 10-4	75
S105-1	19.2	64.8	1.34 x 10-2	0
	20.8	65.0	1.15 x 10-2	10
	21.2	65.0	9.39 x 10-3	20
	24.1	65.1	6.75 x 10-3	30
	21.6	65.4	3.96 x 10-3	40
S106-1	337.4	64.4	7.76 x 10-3	0
	340.1	63.9	4.57 x 10-3	10
	341.7	63.4	2.78 x 10-3	20
	340.8	62.6	1.67 x 10-3	30
	335.2	62.4	1.06 x 10-3	40
	329.6	61.5	7.85 x 10-4	50
	329.6	60.3	6.00 x 10-4	60
S107-1	309.5	48.4	1.67 x 10-3	0
	348.1	59.9	8.30 x 10-4	10
	352.6	58.4	5.87 x 10-4	20
	354.6	56.8	3.51 x 10-4	30
	352.2	58.8	2.03 x 10-4	40
	352.0	56.0	1.22 x 10-4	50
S108-1	330.8	57.1	3.55 x 10-3	0
	345.7	63.9	1.60 x 10-3	10
	345.8	60.8	1.30 x 10-3	20
	344.3	60.8	8.37 x 10-4	30
	345.9	60.8	4.85 x 10-4	40
S109-1	343.4	62.9	4.89 x 10-3	0
	347.8	57.4	2.84 x 10-3	10
	347.9	56.9	2.06 x 10-3	20
	346.5	56.9	1.46 x 10-3	30
	344.7	57.4	1.07 x 10-3	40
	341.5	57.4	8.19 x 10-4	50
	338.3	57.9	6.71 x 10-4	60
S110-1	347.6	58.7	8.64 x 10-3	0
	354.2	59.4	4.51 x 10-3	10
	354.6	58.0	2.74 x 10-3	20
	353.6	58.7	1.63 x 10-3	30
	349.5	58.0	1.03 x 10-3	40
	347.9	60.4	7.39 x 10-4	50
L001-1*	44.1	73.6	1.58 x 10-3	0
	19.9	64.6	8.81 x 10-4	10
	16.7	63.3	6.45 x 10-4	15
	17.0	63.2	6.19 x 10-4	15
	18.2	63.9	4.73 x 10-4	20
	17.3	62.9	3.53 x 10-4	25
	5.4	59.9	2.08 x 10-4	35
	16.6	63.1	2.07 x 10-4	35
	12.6	62.7	1.24 x 10-4	45
	13.6	62.7	1.21 x 10-4	45
	12.8	61.5	8.60 x 10-5	55
	7.6	63.3	6.42 x 10-5	65
	4.8	63.4	4.93 x 10-5	75
	5.3	62.9	5.04 x 10-5	75
L002-0	8.2	73.9	1.62 x 10-3	0
	359.5	64.7	1.36 x 10-3	10
	356.5	63.6	1.10 x 10-3	15
	357.3	64.3	1.01 x 10-3	20

Sample	Declination	Inclination	Intensity (emu/cc)	Demagnetization (mT)
	354.5	62.1	7.18 x 10-4	30
	353.6	60.3	7.08 x 10-4	30
	357.8	65.5	4.04 x 10-4	50
	355.6	64.4	3.94 x 10-4	50
	354.5	61.1	3.19 x 10-4	60
	352.7	60.9	2.80 x 10-4	75
L003-1	288.2	78.3	1.13 x 10-3	0
	359.8	69.8	7.53 x 10-4	10
	357.9	69.6	5.65 x 10-4	15
	357.9	67.6	4.09 x 10-4	20
	358.1	63.7	2.37 x 10-4	30
	357.9	65.8	2.34 x 10-4	30
L004-1	41.3	59.4	1.54 x 10-3	0
	23.2	63.9	9.00 x 10-4	10
	18.8	63.9	6.89 x 10-4	15
	15.9	63.7	5.33 x 10-4	20
	18.4	64.3	5.16 x 10-4	20
	17.7	63.9	3.21 x 10-4	30
L005-1	352.1	70.2	1.87 x 10-3	0
	15.3	66.7	9.97 x 10-4	10
	16.8	68.9	7.97 x 10-4	15
	17.1	65.4	5.81 x 10-4	20
	17.0	67.6	3.73 x 10-4	30
L006-1	96.3	57.8	1.58 x 10-3	0
	29.0	73.4	9.84 x 10-4	10
	20.0	73.4	7.05 x 10-4	15
	18.5	74.5	5.34 x 10-4	20
	9.8	71.8	3.84 x 10-4	25
	11.8	73.2	3.70 x 10-4	25
	15.2	73.6	3.06 x 10-4	30
	17.4	74.7	3.04 x 10-4	30
	13.3	72.0	2.86 x 10-4	30
L007-1	18.5	40.4	2.79 x 10-3	0
	18.4	53.5	1.41 x 10-3	10
	16.2	57.9	1.01 x 10-3	15
	18.2	60.6	7.82 x 10-4	20
	15.7	60.2	7.67 x 10-4	20
	12.3	61.9	5.00 x 10-4	30
	12.4	61.6	4.92 x 10-4	30
	12.3	62.3	4.70 x 10-4	30
	11.8	62.4	3.50 x 10-4	40
	1.5	60.9	2.36 x 10-4	60
	353.2	62.2	2.21 x 10-4	60
L014-1*	22.5	34.1	1.12 x 10-3	0
	22.9	36.0	1.04 x 10-3	10
	24.9	33.3	9.92 x 10-4	15
	24.4	33.9	8.86 x 10-4	20
	24.8	32.7	7.93 x 10-4	25
	24.9	32.6	6.04 x 10-4	35
	25.6	33.4	4.36 x 10-4	45
	25.7	35.1	3.30 x 10-4	55
	27.7	38.4	1.99 x 10-4	75
L015-1	21.5	22.7	9.95 x 10-4	0
	25.1	23.8	9.62 x 10-4	10
	25.5	23.3	8.23 x 10-4	20
	27.6	20.0	6.20 x 10-4	30
	27.3	19.4	4.63 x 10-4	40
	28.5	22.5	3.56 x 10-4	50
	30.6	28.3	2.46 x 10-4	65
	30.1	28.7	2.45 x 10-4	65
	22.8	32.9	2.20 x 10-4	75

Sample	Declination	Inclination	Intensity (emu/cc)	Demagnetization (mT)
L016-1	29.0	22.4	1.32 x 10-3	0
	29.5	18.6	1.29 x 10-3	5
	28.9	19.0	1.26 x 10-3	10
	30.3	17.2	1.09 x 10-3	20
	33.1	9.5	8.49 x 10-4	30
	33.9	0.7	6.46 x 10-4	40
	34.9	-2.5	4.89 x 10-4	50
	32.1	3.7	3.49 x 10-4	60
	31.8	12.1	2.62 x 10-4	70
	27.9	19.4	1.98 x 10-4	80
L017-1	29.8	31.4	7.19 x 10-4	0
	31.8	18.5	7.99 x 10-4	5
	32.6	17.7	7.78 x 10-4	10
	32.3	16.7	6.77 x 10-4	20
	32.6	14.9	5.59 x 10-4	30
	33.1	12.4	4.50 x 10-4	40
	33.7	9.0	3.65 x 10-4	50
	35.9	6.0	2.67 x 10-4	60
	40.1	21.1	1.27 x 10-4	70
	47.3	18.0	7.62 x 10-5	80
L018-1	15.8	45.1	7.11 x 10-4	0
	27.7	20.7	6.51 x 10-4	5
	27.2	16.2	5.82 x 10-4	10
	28.8	13.3	4.90 x 10-4	20
	29.3	10.4	4.01 x 10-4	30
	30.6	8.1	3.27 x 10-4	40
	30.2	6.9	2.58 x 10-4	50
	31.7	3.2	2.10 x 10-4	60
	35.0	-2.7	1.79 x 10-4	70
	34.9	-6.8	1.46 x 10-4	80
L028-1*	20.6	63.9	5.53 x 10-3	0
	22.4	64.6	5.02 x 10-3	5
	22.0	65.2	4.22 x 10-3	10
	20.6	65.6	2.63 x 10-3	20
	19.6	65.8	1.61 x 10-3	30
	18.5	65.4	1.05 x 10-3	40
	19.2	65.8	7.08 x 10-4	50
	18.3	65.6	5.09 x 10-4	60
	19.2	65.1	3.67 x 10-4	70
	17.1	66.1	3.20 x 10-4	80
L029-1	15.3	67.0	5.18 x 10-3	0
	22.6	66.3	4.79 x 10-3	5
	24.0	66.3	4.22 x 10-3	10
	23.4	67.1	2.92 x 10-3	20
	22.9	67.8	1.75 x 10-3	30
	22.5	68.5	5.99 x 10-4	50
	21.6	68.8	2.99 x 10-4	70
L030-1	8.5	62.1	4.53 x 10-3	0
	15.4	64.7	4.04 x 10-3	5
	18.8	65.8	3.18 x 10-3	10
	18.4	65.7	1.59 x 10-3	20
	15.8	65.8	7.28 x 10-4	30
	13.4	64.8	3.49 x 10-4	40
	9.6	65.0	1.89 x 10-4	50
	10.1	65.2	1.90 x 10-4	50
L031-1	2.2	61.0	3.46 x 10-3	0
	8.6	65.9	2.52 x 10-3	5
	9.5	66.0	2.46 x 10-3	5
	15.2	66.7	1.67 x 10-3	10
	15.8	66.3	8.10 x 10-4	20
	12.8	66.4	4.26 x 10-4	30

Sample	Declination	Inclination	Intensity (emu/cc)	Demagnetization (mT)
	12.4	66.6	2.34 x 10-4	40
	359.5	65.3	1.48 x 10-4	50
	3.1	63.6	1.49 x 10-4	50
	354.9	57.9	9.55 x 10-5	60
	350.1	62.3	5.53 x 10-5	80
L032-0	6.2	55.0	2.46 x 10-3	0
	11.6	59.6	1.56 x 10-3	5
	14.4	60.7	8.97 x 10-4	10
	13.4	61.4	4.70 x 10-4	20
	10.0	61.0	2.87 x 10-4	30
	6.9	61.2	1.41 x 10-4	50
	11.2	62.0	1.38 x 10-4	50
	14.6	61.2	6.87 x 10-5	70
	18.5	61.8	5.29 x 10-5	80
L033-1	8.4	57.0	3.69 x 10-3	0
	11.8	62.6	2.39 x 10-3	5
	13.5	65.5	1.27 x 10-3	10
	13.1	65.9	5.88 x 10-4	20
	7.0	64.7	3.61 x 10-4	30
	14.7	64.6	1.79 x 10-4	50
	14.8	66.4	1.65 x 10-4	50
	15.0	66.7	9.49 x 10-5	70
	13.8	68.2	8.06 x 10-5	80
L034-1*	302.6	66.0	2.19 x 10-3	0
	316.6	69.4	1.57 x 10-3	10
	318.1	69.8	1.32 x 10-3	15
	319.0	69.9	1.12 x 10-3	20
	318.1	70.4	8.24 x 10-4	30
	318.9	70.4	5.84 x 10-4	40
	316.0	69.9	4.03 x 10-4	50
	326.7	69.0	2.41 x 10-4	65
	326.5	69.1	1.83 x 10-4	75
L035-1	274.6	46.4	1.15 x 10-3	0
	293.7	63.4	3.64 x 10-4	10
	294.7	61.3	1.31 x 10-4	20
	307.5	62.3	1.20 x 10-4	20
	312.0	63.6	6.87 x 10-5	30
	313.0	66.9	6.66 x 10-5	30
	319.9	59.2	4.41 x 10-5	40
	322.2	63.2	4.62 x 10-5	40
	316.5	61.3	4.69 x 10-5	40
	321.1	62.9	4.47 x 10-5	40
L036-1	317.5	66.7	1.84 x 10-3	0
	305.3	69.3	5.20 x 10-4	10
	306.2	68.6	3.31 x 10-4	15
	307.9	69.4	2.16 x 10-4	20
L037-1	338.8	65.2	2.42 x 10-3	0
	328.6	70.5	5.34 x 10-4	10
	322.5	70.8	3.43 x 10-4	15
	325.9	72.8	2.12 x 10-4	20
	323.2	72.3	1.66 x 10-4	25
	321.8	72.9	1.74 x 10-4	25
L038-0	311.0	61.9	2.53 x 10-3	0
	319.7	69.8	8.53 x 10-4	10
	317.7	69.4	5.66 x 10-4	15
	316.5	70.0	3.94 x 10-4	20
	314.1	70.8	2.89 x 10-4	25
	313.5	70.0	2.82 x 10-4	25
L039-1	3.6	73.2	2.47 x 10-3	0
	344.6	72.4	5.44 x 10-4	10
	327.2	73.4	3.19 x 10-4	15

Sample	Declination	Inclination	Intensity (emu/cc)	Demagnetization (mT)
	318.2	74.3	2.29 x 10-4	20
	325.7	74.1	2.18 x 10-4	20
	323.3	75.2	1.58 x 10-4	25
	316.6	71.9	1.32 x 10-4	30
	319.1	72.5	1.19 x 10-4	35
	313.3	70.9	1.19 x 10-4	35
L040-1*	79.2	69.6	2.48 x 10-3	0
	132.6	63.9	1.16 x 10-3	10
	134.6	61.1	7.44 x 10-4	15
	133.1	61.4	4.44 x 10-4	20
	134.8	60.5	1.74 x 10-4	30
	128.4	60.6	6.04 x 10-5	45
	130.1	63.2	6.32 x 10-5	45
	139.8	57.8	2.72 x 10-5	60
	108.9	43.1	3.32 x 10-5	60
L041-0	67.0	79.5	2.05 x 10-3	0
	127.3	63.3	7.73 x 10-4	10
	132.0	64.8	4.30 x 10-4	15
	133.7	63.3	2.38 x 10-4	20
	133.0	60.8	1.59 x 10-4	25
	125.8	60.9	1.06 x 10-4	30
	123.8	66.7	6.36 x 10-5	40
	124.7	62.0	6.54 x 10-5	40
	140.6	48.8	5.79 x 10-5	40
	154.6	54.4	3.15 x 10-5	60
	164.1	51.0	2.85 x 10-5	60
	130.7	62.8	3.37 x 10-5	60
	100.7	45.8	2.74 x 10-5	60
L042-1	12.8	57.8	2.02 x 10-3	0
	113.0	70.6	4.51 x 10-4	10
	116.1	68.0	3.39 x 10-4	15
	122.1	68.3	1.27 x 10-4	20
	131.8	68.5	8.78 x 10-5	25
	119.1	62.6	9.33 x 10-5	25
	149.2	72.1	7.59 x 10-5	25
L043-0	18.3	84.6	3.92 x 10-3	0
	62.1	75.3	1.16 x 10-3	10
	70.3	75.5	8.76 x 10-4	15
	83.8	74.9	7.00 x 10-4	20
	86.2	75.0	5.91 x 10-4	25
	98.8	72.6	4.93 x 10-4	30
	95.7	74.1	4.92 x 10-4	30
	103.8	74.2	3.91 x 10-4	40
	110.2	76.1	3.17 x 10-4	50
	116.3	75.7	3.04 x 10-4	50
	134.1	73.8	2.48 x 10-4	60
	137.3	75.5	2.42 x 10-4	60
	157.0	69.7	2.00 x 10-4	70
L044-1	51.1	61.5	3.23 x 10-3	0
	69.2	74.3	9.67 x 10-4	10
	73.9	75.4	7.33 x 10-4	15
	83.3	76.2	5.90 x 10-4	20
	85.0	75.4	5.20 x 10-4	25
	86.3	75.4	4.33 x 10-4	30
	95.0	76.3	3.53 x 10-4	40
	84.6	75.0	3.43 x 10-4	40
L045-1	11.6	41.0	2.58 x 10-3	0
	27.5	65.7	1.35 x 10-3	10
	31.7	70.5	9.46 x 10-4	20
	40.5	72.4	8.31 x 10-4	25
	35.2	73.4	7.04 x 10-4	35

Sample	Declination	Inclination	Intensity (emu/cc)	Demagnetization (mT)
	28.4	72.9	6.47 x 10-4	40
	31.7	72.9	6.26 x 10-4	40
	30.1	72.7	6.25 x 10-4	40
	36.1	73.7	5.24 x 10-4	50
L046-0	12.9	47.5	3.70 x 10-3	0
	57.7	73.6	4.13 x 10-4	10
	74.5	74.0	2.53 x 10-4	15
	74.9	73.9	2.49 x 10-4	15
	86.6	74.3	1.80 x 10-4	20
	99.4	72.3	1.53 x 10-4	25
	120.7	67.2	1.03 x 10-4	35
	131.3	76.5	7.22 x 10-5	45
	111.3	72.9	8.01 x 10-5	45
	130.8	73.3	7.85 x 10-5	50
	96.0	65.9	7.33 x 10-5	60
L053-1*	194.6	-58.8	2.06 x 10-3	0
	195.0	-58.0	2.73 x 10-3	10
	194.1	-57.8	2.60 x 10-3	15
	193.7	-57.7	2.34 x 10-3	20
	193.6	-57.4	1.66 x 10-3	30
	193.6	-57.6	1.05 x 10-3	40
	190.7	-58.4	3.97 x 10-4	60
	190.6	-56.1	1.97 x 10-4	75
L054-0	127.0	-16.2	1.15 x 10-3	0
	185.6	-65.3	9.41 x 10-4	10
	194.2	-66.7	7.75 x 10-4	15
	193.9	-66.5	6.13 x 10-4	20
	187.0	-64.8	3.95 x 10-4	30
	194.6	-67.3	3.94 x 10-4	30
L055-0	115.1	14.7	9.70 x 10-4	0
	190.8	-66.8	1.39 x 10-3	10
	193.6	-66.8	1.25 x 10-3	15
	197.2	-66.9	1.07 x 10-3	20
	195.5	-66.6	8.91 x 10-4	25
	196.4	-66.9	7.58 x 10-4	30
L056-1	159.1	-57.1	1.89 x 10-3	0
	191.8	-63.5	2.16 x 10-3	10
	187.1	-64.1	1.74 x 10-3	15
	194.0	-64.0	1.48 x 10-3	20
	194.0	-63.4	1.18 x 10-3	25
	195.5	-62.7	9.30 x 10-4	30
L057-1	172.7	-61.3	1.92 x 10-3	0
	191.9	-62.6	2.29 x 10-3	10
	192.4	-62.5	2.03 x 10-3	15
	194.5	-62.3	1.60 x 10-3	20
	193.8	-62.9	1.56 x 10-3	20
L058-1	180.3	-72.7	9.38 x 10-4	0
	186.0	-71.3	9.83 x 10-4	10
	193.2	-69.9	1.04 x 10-3	15
	187.9	-71.0	9.95 x 10-4	20
	200.6	-67.9	1.06 x 10-3	25
	187.8	-70.9	8.77 x 10-4	30
	193.4	-69.9	8.21 x 10-4	35
	197.8	-69.5	6.97 x 10-4	40
	193.3	-70.1	6.63 x 10-4	40
L059-1	191.3	-68.8	1.37 x 10-2	0
	192.5	-68.9	1.37 x 10-2	10
	192.9	-68.9	1.33 x 10-2	15
	194.0	-69.0	1.10 x 10-2	25
	194.2	-69.2	6.88 x 10-3	35
L060-1*	35.8	65.6	4.65 x 10-4	0

Sample	Declination	Inclination	Intensity (emu/cc)	Demagnetization (mT)
	88.9	-30.2	1.64 x 10-4	10
	73.3	-48.9	1.84 x 10-4	15
	75.4	-55.4	1.86 x 10-4	20
	76.6	-60.6	1.67 x 10-4	30
	78.9	-62.9	1.41 x 10-4	40
	79.2	-64.8	1.14 x 10-4	50
	80.7	-63.9	1.11 x 10-4	50
	81.1	-63.9	1.12 x 10-4	50
	76.5	-62.8	8.71 x 10-5	60
	79.3	-66.5	5.09 x 10-5	75
L061-1	188.4	42.2	3.18 x 10-4	0
	97.7	-50.7	9.72 x 10-5	10
	81.4	-59.1	1.09 x 10-4	20
	76.9	-60.2	9.63 x 10-5	30
	78.5	-57.8	7.70 x 10-5	40
	74.3	-61.7	6.80 x 10-5	50
	80.2	-59.2	4.77 x 10-5	60
L062-1	89.3	67.1	4.05 x 10-4	0
	70.0	-22.5	1.22 x 10-4	10
	69.0	-57.2	7.99 x 10-5	40
	64.5	-60.2	6.20 x 10-5	50
	76.1	-61.6	4.72 x 10-5	60
	71.3	-62.6	4.64 x 10-5	60
L063-1	269.3	29.6	3.13 x 10-4	0
	42.2	-68.8	1.54 x 10-4	10
	55.6	-64.7	1.34 x 10-4	20
	58.6	-66.3	8.95 x 10-5	30
	58.7	-66.2	5.52 x 10-5	40
L064-1	263.3	40.1	4.25 x 10-4	0
	344.8	-69.9	6.83 x 10-5	10
	37.4	-70.5	4.56 x 10-5	30
	49.4	-72.7	2.72 x 10-5	40
	54.8	-73.2	2.47 x 10-5	50
	50.6	-65.8	2.28 x 10-5	60
	71.5	-65.4	2.26 x 10-5	60
L066-1*	21.7	61.6	3.24 x 10-3	0
	22.0	60.2	2.71 x 10-3	10
	20.9	59.5	2.01 x 10-3	20
	20.1	59.9	1.35 x 10-3	30
	18.7	60.1	8.52 x 10-4	40
	18.2	59.7	5.53 x 10-4	50
	19.5	59.9	3.65 x 10-4	60
	22.6	58.8	2.59 x 10-4	70
L067-1	12.1	62.0	4.09 x 10-3	0
	13.8	61.0	3.63 x 10-3	10
	14.1	60.6	2.83 x 10-3	20
	13.7	60.1	2.00 x 10-3	30
L068-1	16.8	65.5	3.34 x 10-3	0
	17.5	63.1	2.66 x 10-3	10
	16.7	62.6	1.92 x 10-3	20
	16.8	62.3	1.28 x 10-3	30
L069-1	24.3	64.9	2.06 x 10-3	0
	21.8	63.5	9.07 x 10-4	10
	21.5	61.9	5.72 x 10-4	15
	22.4	60.2	4.13 x 10-4	20
	17.2	59.2	2.51 x 10-4	30
	16.7	59.5	2.28 x 10-4	30
	17.1	61.1	1.59 x 10-4	40
	21.5	59.2	1.44 x 10-4	40
	24.0	60.0	1.35 x 10-4	40
	21.2	59.6	9.16 x 10-5	50

Sample	Declination	Inclination	Intensity (emu/cc)	Demagnetization (mT)
L070-1	359.0	64.5	2.58 x 10-3	0
	12.1	60.4	1.18 x 10-3	10
	13.2	60.2	8.62 x 10-4	15
	13.6	59.3	6.62 x 10-4	20
L071-1	6.3	56.6	3.61 x 10-3	0
	9.6	54.7	3.02 x 10-3	10
	10.1	54.3	2.67 x 10-3	15
	10.5	54.3	2.33 x 10-3	20
	11.4	54.0	1.72 x 10-3	30
	11.4	54.1	1.14 x 10-3	40
L072-0*	49.8	38.1	8.57 x 10-4	0
	38.8	62.0	2.07 x 10-4	10
	32.8	60.2	1.38 x 10-4	15
	29.6	60.8	8.49 x 10-5	20
	28.0	61.2	5.76 x 10-5	25
	26.7	57.5	3.50 x 10-5	30
	34.4	57.1	3.42 x 10-5	30
	37.3	56.1	2.27 x 10-5	40
	18.2	65.8	2.21 x 10-5	40
L073-1	104.1	36.9	7.25 x 10-4	0
	61.7	67.1	1.94 x 10-4	10
	49.8	67.4	7.02 x 10-5	20
	46.2	66.2	5.21 x 10-5	25
	36.5	65.4	4.44 x 10-5	25
	39.9	67.0	3.25 x 10-5	30
	25.3	64.8	3.30 x 10-5	30
	35.7	65.8	2.16 x 10-5	40
	42.0	66.0	2.08 x 10-5	40
L074-1	52.3	8.1	6.33 x 10-4	0
	39.8	42.4	2.35 x 10-4	10
	36.4	49.2	1.44 x 10-4	15
	36.0	51.4	9.25 x 10-5	20
	33.6	54.5	8.98 x 10-5	20
	32.8	52.1	6.73 x 10-5	25
	30.9	56.3	6.00 x 10-5	25
	27.4	53.5	3.76 x 10-5	30
	29.5	51.9	3.68 x 10-5	30
	26.8	51.7	3.15 x 10-5	35
	28.8	62.5	3.12 x 10-5	35
	15.2	69.7	2.02 x 10-5	45
	25.4	73.8	2.27 x 10-5	45
L075-1	80.8	62.8	1.28 x 10-3	0
	57.1	65.2	3.72 x 10-4	10
	47.7	65.8	2.09 x 10-4	15
	42.1	66.6	1.31 x 10-4	20
	43.2	65.8	9.42 x 10-5	25
	40.0	67.5	6.66 x 10-5	30
	39.3	68.5	5.08 x 10-5	35
	27.4	63.0	4.02 x 10-5	40
	18.4	72.9	2.32 x 10-5	60
	25.1	72.6	1.87 x 10-5	75
L076-1	57.8	8.6	6.66 x 10-4	0
	65.5	41.7	1.65 x 10-4	10
	65.6	51.8	6.26 x 10-5	20
	64.6	54.5	3.81 x 10-5	25
	67.9	55.8	3.35 x 10-5	30
	101.2	66.4	2.39 x 10-5	40
	68.0	80.1	1.82 x 10-5	50
	86.7	62.5	1.59 x 10-5	60
	105.8	57.6	1.54 x 10-5	75
	134.3	73.0	1.25 x 10-5	75

Sample	*Declination*	*Inclination*	*Intensity (emu/cc)*	*Demagnetization (mT)*
L077-1	36.0	47.5	1.18 x 10-3	0
	34.1	58.8	3.60 x 10-4	10
	34.1	62.6	2.13 x 10-4	15
	31.3	62.2	2.11 x 10-4	15
	34.6	62.4	1.39 x 10-4	20
	36.0	64.9	9.94 x 10-5	25
	39.7	64.5	7.30 x 10-5	30
	41.2	67.1	6.51 x 10-5	35
	23.8	61.5	4.32 x 10-5	40
	24.2	68.2	3.49 x 10-5	50
	27.0	69.3	3.06 x 10-5	60
	26.9	66.8	2.26 x 10-5	60
L078-0*	339.5	68.9	3.25 x 10-3	0
	336.2	66.5	2.76 x 10-3	10
	334.6	65.0	2.34 x 10-3	15
	334.0	64.6	1.99 x 10-3	20
	332.5	64.0	1.45 x 10-3	30
	333.1	63.3	9.87 x 10-4	40
	332.4	60.9	7.08 x 10-4	50
	330.5	59.7	4.92 x 10-4	60
	330.2	61.4	3.65 x 10-4	75
L079-1	351.3	67.8	3.98 x 10-3	0
	345.1	67.1	2.91 x 10-3	10
	346.5	65.5	1.92 x 10-3	20
	344.0	65.7	1.22 x 10-3	30
	342.7	66.0	7.80 x 10-4	40
	337.7	66.5	3.53 x 10-4	60
L080-1	353.7	66.7	3.07 x 10-3	0
	349.6	65.1	2.37 x 10-3	10
	345.6	64.8	1.58 x 10-3	20
	344.3	63.2	1.08 x 10-3	30
	340.8	63.2	7.31 x 10-4	40
	341.8	62.9	5.28 x 10-4	50
	338.6	64.4	3.76 x 10-4	60
	337.8	64.5	3.82 x 10-4	60
L081-1	330.1	62.8	4.15 x 10-3	0
	332.5	62.5	3.27 x 10-3	10
	332.8	62.2	2.08 x 10-3	20
	332.4	62.1	1.37 x 10-3	30
L082-1	319.5	76.6	2.71 x 10-3	0
	321.9	73.0	2.09 x 10-3	10
	325.6	70.2	1.34 x 10-3	20
	324.4	69.1	8.91 x 10-4	30
	325.4	67.3	5.93 x 10-4	40
	328.1	65.3	4.12 x 10-4	50
L083-1	335.5	62.2	3.59 x 10-3	0
	335.5	62.2	2.85 x 10-3	10
	335.0	62.2	1.88 x 10-3	20
	334.8	62.4	1.24 x 10-3	30
L084-1	62.1	63.2	1.54 x 10-3	0
	10.0	65.3	6.94 x 10-4	10
	356.1	62.5	3.68 x 10-4	20
	348.5	58.6	2.29 x 10-4	30
	342.5	59.7	1.64 x 10-4	40
	342.1	59.2	1.14 x 10-4	50
	339.1	61.2	8.30 x 10-5	60
	342.0	59.9	5.35 x 10-5	70

Paleomagnetic samples are listed according to site with the first sample of each site denoted by an (*) after the sample number. As in Table 1 the sites

from the northern sample locality have S sample numbers and sites from the southern sample locality have L sample numbers. The last column labeled ***Demagnetization*** (*mT*) notes the magnetic cleaning field in milliteslas for each measurement.

Appendix 2. Map projections

The computer-generated maps of this paper were constructed using the following projections --

Polar equal area (Lambert), map center 41°N,240°E: Figures 1, 13, 16, 17, 18, 19, 20.

Polar equal area (Lambert), map center 45.5°N,238°E: Figure 2.

Polar equal area (Lambert), map center 41°N,260°E: Figure 3a

Polar equal area (Lambert), map center 41°N,230°E: Figure 3b

Lambert conformal conic, standard parallels 60°N and 40°N, central meridian 230°E: Figure 21.